Synthesis, structure and properties of metal nanoclusters†

J. P. Wilcoxon*[a] and B. L. Abrams[b]

Metal nanoclusters have physical properties differing significantly from their bulk counterparts. Metallic properties such as delocalization of electrons in bulk metals which imbue them with high electrical and thermal conductivity, light reflectivity and mechanical ductility may be wholly or partially absent in metal nanoclusters, while new properties develop. We review modern synthetic methods used to form metal nanoclusters. The focus of this *critical review* is solution based chemical synthesis methods which produce fully dispersed clusters. Control of cluster size and surface chemistry using inverse micelles is emphasized. Two classes of metals are discussed, transition metals such as Au and Pt, and base metals such as Co, Fe and Ni. The optical and catalytic properties of the former are discussed and the magnetic properties of the latter are given as examples of unexpected new size-dependent properties of nanoclusters. We show how classical surface science methods of characterization augmented by chemical analysis methods such as liquid chromatography can be used to provide feedback for improvements in synthetic protocols. Characterization of metal clusters by their optical, catalytic, or magnetic behavior also provides insights leading to improvements in synthetic methods. The collective physical properties of closely interacting clusters are reviewed followed by speculation on future technical applications of clusters. (125 references).

Introduction

This review emphasizes small metal nanoclusters (>1–10 nm in size) which compose the size regime between the molecular and solid state. With a decrease in metal cluster size, their

[a] *Department of Physics, University of Birmingham, Birmingham, U.K.. E-mail: jpwilco@gmail.com*
[b] *Center for Individual Nanoparticle Functionality (CINF), NanoDTU, Dept of Physics, Technical University of Denmark, DK-2800 Kongens Lyngby, Denmark. E-mail: babrams03@gmail.com*
† The HTML version of this article has been enhanced with colour images.

abundant surface begins to play a dominant role providing a unique way to learn how metal–metal bonding, cluster shape, and packing are affected by ligands bound to the cluster surface. We review studies which provide insights into complex issues in catalysis, such as selectivity of binding of substrates to vertex, edge, or face sites on a metal cluster and how such binding affects the intermetal bond distances. These binding effects often result in a surface reconstruction, mass redistribution, or cluster shape change. Studies of 3-D interface structural changes in nanosize metal clusters should yield information quite different from the extensive literature

J. P. Wilcoxon

Dr Wilcoxon obtained his doctorate in physical chemistry from the University of Washington in 1983 and has worked in the areas of nanocluster synthesis and characterization since 1988. At Sandia National Laboratories, his research interests in the phase behavior of micellar systems and cluster growth processes led to the development of inverse micelle methods for metal nanocluster formation. He developed the application of size-exclusion chromatography to quantify the size-dependent optical properties of metal clusters. His current research interests emphasize the use of metal and semiconductor clusters as novel catalysts with application in energy and environmental technologies.

B. L. Abrams

Dr Abrams graduated with her PhD in Materials Science and Engineering from the University of Florida, Gainesville, Florida in December of 2001. As part of her graduate studies she analyzed the effects of the surface on luminescent properties of semiconductor phosphors under the guidance of Professor Paul Holloway. Following her graduate studies, Billie began working as a postdoctoral associate in the area of nanocluster synthesis and characterization with Dr Jess Wilcoxon at Sandia National Laboratories. Her work focused on investigating interfacial and surface chemical interactions of the nanoclusters with their environment for applications in catalysis and photocatalysis for renewable energy along with some applications in luminescent materials, magnetism, and radiation detection.

describing ligand interactions with extended, 2-D metal surfaces. Cluster studies require the development of new characterization tools to complement those of traditional surface science which require high vacuum conditions. For example, the optical properties of metal clusters in a vacuum differ substantially from those found in dispersed solutions. Since clusters more closely resemble practical heterogeneous catalysts important new scientific and technical insights may be gained by their investigation.

The chemical research literature concerning synthesis and characterization of metal clusters is extensive but this review only focuses on liquid phase chemical methods for formation of clusters in the important 1–10 nm size regime where cluster surface properties play a dominant role. The review thus excludes work concerning classical colloidal synthesis methods in aqueous solution which generally produce larger, more polydisperse clusters. In this colloidal regime kinetics plays a dominant role in the colloid growth leading to substantial size and shape polydispersity for most metal colloids. There are many good reviews in this area such as those by Liz-Marzan *et al.* and references therein.[1,2]

A key limitation of colloidal synthesis in aqueous solution is that the water phase may react with many types of strong chemical reductants required to reduce transition metal ion precursors. So, the emphasis of this review on cluster formation in non-polar solvents containing stabilizing ligands is motivated by the large variety of metal clusters which may be formed with good size control and complete homogeneous dispersion in an organic continuous phase. Complete cluster dispersion is critical to the interpretation of most characterization studies which include size-dependent optical, catalytic, and magnetic measurements.

We also exclude from our discussion gas phase methods and vacuum approaches to cluster formation since such processes generally produce aggregates of individual clusters whose physical properties such as optical absorbance are complex due to strong sintering between clusters. This is a fundamental limitation of these formation methods since there are no surfactants present during the atomic aggregation and cluster growth stages. Thus, individual metal clusters will sinter or fuse with other clusters in most cases. An additional limitation of such methods is the nearly three orders of magnitude reduction in atomic concentration in the gas phase, which limits the number density of clusters formed and thus the types of experimental characterization approaches such as optical absorption. These optical and magnetic characterization methods rely on dilute, fully dispersed clusters which are only available for surfactant-stabilized clusters formed in solution. However, there exist some excellent reviews in this area as well.[3]

The development of synthetic protocols for organic chemical and/or cluster synthesis is highly dependent on reliable, rapid, and general characterization methods. For example, the combination of gas chromatography with mass spectrometry has been critical for identifying the products, (and unwanted by-products), of organic synthesis. When combined with traditional elemental analysis such as nuclear magnetic resonance (NMR) and Fourier transform infra-red spectroscopy (FTIR), a complete picture of the organic product is possible. In the area of biopolymers and polymers, liquid chromatography and capillary gel electrophoresis coupled to new detector technologies such as laser desorption, time-of-flight mass spectrometry and electrospray mass spectrometry has accelerated the analysis of proteins, DNA, RNA and polymers in general.

Characterization and feedback for the development of cluster synthesis is in a more nascent state than for the case of organic or polymer chemistry. It is rarely possible, for example, to perform elemental or structural analysis on individual clusters since high spatial resolution is difficult to achieve non-destructively and, furthermore, a sufficient number of clusters must be counted to give statistical significance for the population as a whole. For serial analysis methods like electron microscopy acceptable statistics based upon the entire grid area cannot be obtained. Instead, techniques such as selected area electron diffraction which sample and average over large areas yield an ensemble average structure for the as-synthesized sub-population of clusters in the analysis region. This includes any non-volatile by-products (*e.g.* salts) from the synthesis. Traditional size, shape, and composition determinations of clusters deposited on grids and studied in high vacuum include X-ray photoelectron spectroscopy (XPS), transmission electron microscopy (TEM), and X-ray diffraction (XRD). Their utility and limitations will be briefly discussed in this review. Our review will emphasize characterization and analysis techniques combining rapid cluster size, shape, and composition based cluster separation for an entire population of as-synthesized clusters.

The key element lacking in traditional surface science methods applied to cluster characterization is the ability to separate and discriminate separate sub-populations of clusters and then analyze them. There is also the possibility of altering the shape or cluster chemistry when the clusters are introduced into the vacuum. Since obtaining a dispersed particle beam of clusters in a gas phase is usually impossible, mass spectroscopic analysis is very difficult. Most cluster synthesis occurs in liquid phase for reasons to be discussed and our review focuses on characterization methods which allow clusters to be studied in their native, dispersed state in solution. As in the case of high molecular weight organic chemical synthesis, liquid chromatography, specifically size exclusion chromatography (SEC), is best suited for cluster characterization in solution.

Background

Historically, metal colloids were the first nanosize inorganic particles to be scientifically investigated. For example, formation of metal colloids or clusters by the controlled reduction, nucleation, and growth from metal salts in aqueous solution has been studied for over a century. The earliest scientific investigations of gold colloids were undertaken by Michael Faraday and spanned over a decade.[4] As pointed out by Kreibig and Vollmer in their excellent review of the optical properties of metal clusters human interest in the colors of metal-based colloidal systems dates to the Roman times.[5] A Roman goblet from the 4th Century in the British museum whose fame is due to the shining colors generated by a composition of Ag and Au clusters is just one example cited.

This journal is © The Royal Society of Chemistry 2006

Chem. Soc. Rev., 2006, **35**, 1162–1194 | 1163

The association of purple with royal colors is thought to be due to the purple colors arising from colloidal Au and Cu dispersions.[5]

The Faraday method of colloidal synthesis is based upon the chemical reduction of suitably chosen precursor metal salts in an aqueous solution. These wine-red sols exhibited remarkable stability due to charge stabilization *via* adsorbed citrate ions. This stability is demonstrated by the fact that samples prepared in sealed vials by Faraday in the mid 1850s can still be viewed in the Cavendish museum in Cambridge. However, this general method, even with its modern refinements is not easily extended to other similar metals like Ag or Pt. Nor can a wide range of sizes with narrow polydispersity or high concentrations be easily produced.

Scientists have only recently developed non-aqueous methods of colloidal synthesis utilizing steric, instead of charge, stabilization. Ligands, typically surfactants or amphiphilic polymers are present during the cluster growth and prevent aggregation between clusters by keeping the cluster surfaces apart during collisions in solution. An early example of this approach which ultimately led to the development of magnetic particles for recording purposes was that of Hoon *et al.*[6] They produced Co colloids (now called nanoclusters, nanocrystals, or nanoparticles) in the 1–100 nm range by thermolysis of $Co_2(CO)_8$ in the presence of dispersant polymers. This seminal work provided the basis of nearly all subsequent methods for production of colloids from metal-organic precursors using high T decomposition. Soon after the initial work by Hoon, other reports by Hess *et al.* and Griffiths *et al.* of base metal colloidal synthesis *via* thermal decomposition in the presence of surfactants or polymers emerged.[7,8] More recently, with the advent of exotic organometallic precursors, Murray *et al* synthesized base metal clusters of Co, Fe and Ni using this approach.[9] Extensions of the methods to produce nanoalloys or core/shell particles such as FePt were also described.[10]

Although thermolysis of organometallic precursors is the chemical basis of many current approaches to cluster synthesis in non-aqueous, low-dielectric constant solvents, there are some drawbacks to this approach. The toxicity, air-sensitivity, expense, and unwanted by-products (*e.g.* metallic films) prevent the widespread adoption of such methods outside the chemical community. There are also difficulties with scaling up such methods to safely produce larger quantities of clusters. Finally, most metals do not have suitable metal organic precursors required for practical implementation of this approach for most elements in the periodic table. Thus, metal cluster synthesis methods based upon reduction of ionic metal salt precursors under ambient conditions are more generally useful.

Systematic methods of cluster size control in organometallic decomposition synthesis are somewhat lacking. However, in certain cases remarkable monodispersity can be achieved. One of the earliest and best known examples of monodisperse metal cluster growth from atomic precursors in solution was the synthesis by Schmid[11] (later reviewed by Aiken[12]) of Au(N = 55) clusters by diborane reduction of Au(PPh₃)Cl in benzene or methylene chloride. As represented in Fig. 1, fifty-five atoms in a metal cluster grown from an atomic source corresponds to the closing of the second atomic shell of a Au(N = 13) cluster core with 42 Au atoms and a dozen triphenyl phosphine, PPh₃ molecules weakly ligated to the faces of the inorganic core. This work showed that the role of the ligand is to sterically stabilize inorganic nanoclusters in a solvent and it was critical in determining the eventual structure and stable size of a given nanocluster. Schmid used a continuation of this growth process to extend the available size range to many thousands of atoms, utilizing a synthesis reminiscent of polymeric growth—one generation providing the "seeds" for the next.[13] His approach has also been extended to other metals such as Cu, Pd and Pt.[14] However, the yields from each growth generation are low. Thus, as in organic synthesis, the overall yield can be small for larger clusters. Also, the weak binding of the PPh₃ group means that the long term stability (*e.g.* longer than a few days) of such clusters is severely compromised. TEMs of Au(N = 55), for example, exhibit only larger aggregates of the smaller 55 atom units, likely due to desorption of the labile ligands from the clusters in the TEM vacuum.

Given the limitations outlined above for organometallic routes to metal clusters, a more universal nanocluster synthesis which combines the advantages of low toxicity/cost precursors, and high yield of traditional aqueous based colloidal chemistry with the size dispersion control and chemical versatility of organometallic methods would be quite useful. With this goal in mind Boutonnet, Kizling, and Stenius first used aqueous

Full-Shell "Magic Number" Clusters					
Number of shells	1	2	3	4	5
Number of atoms in cluster	M_{13}	M_{55}	M_{147}	M_{309}	M_{561}
Percentage surface atoms	92%	76%	63%	52%	45%

Fig. 1 Full-shell magic number formation showing how the number of shells relates to the number of atoms in a cluster and the percent of atoms present on the surface. (Reprinted from reference 11: G. Schmid, *Endeavour*, Cluster and Colloids – Bridges Between Molecular and Condensed Material, 1990, **14**, 172. Copyright 1990 with permission from Elsevier and ref 12: J. D. Aiken and R. G. Finke, A review of modern transition-metal nanoclusters: their synthesis, characterization, and applications in catalysis. *J. Mol. Catal. A: Chem.* 1999, **145**(1–2), 1–44. Copyright 1999 with permission from Elsevier.)

pools of water found in oil-continuous microemulsions to solubilize simple ionic metal salts of Au, Pd, Pt, and Rh, followed by chemical reduction using hydrazine or hydrogen gas to produce metal clusters dispersed in oils.[15] Such new nanomaterials were later shown to have good catalytic activity for hydrogenation.[16] Thus, even in this earliest work, characterization *via* catalytic activity provided a useful feedback tool for evaluation of sample quality.

The initial work of Boutonnet *et al.* on synthesis of metal colloids in microemulsions was extended by Pileni and co-workers who employed a widely investigated anionic inverse microemulsion system called AOT to control the cluster growth and stabilize the individual clusters against aggregation.[17–19] Generally, inverse microemulsion synthesis has invoked the concept of a water to surfactant ratio as a control parameter determining the final size of the cluster.[18,20] A general observation supporting this premise is that as more water is solubilized in the microemulsion interior its volume increases and so does the final cluster size. However, microemulsions have greater size dispersion than inverse micelles, and this polydispersity increases with water content so it is also generally found that increases in the water : surfactant ratio result in substantial cluster size polydispersity. This microemulsion method was also later utilized by Steigerwald *et al* during some nucleation and growth studies of semiconductor nanoclusters[21] and there are extensive reviews in this area.[22]

One serious limitation of using water containing microemulsions as microscopic reactors for metal colloid formation was the limited types of reducing agents permitted, (basically hydrazine or aqueous $NaBH_4$). Accompanying the limited chemical variety of reducing agents available is the inherent polydispersity of microemulsions, which results in a broad size dispersion in the final product. These limitations were overcome by the discovery that ionic metal salts could be directly dissolved in a variety of newly discovered inverse micelle systems.[23,24] Inverse micelle systems are defined by the absence of added water and/or air allowing the use of very strong, even pyrophoric, reductants such as $LiAlH_4$ dissolved in tetrahydrofuran, a solvent miscible with most aliphatic and aromatic solvents. This innovation permitted even Si and Ge nanocrystalline clusters to be made by low-T chemical synthesis for the first time.[25,26] In addition, the low polydispersity of inverse micelle systems compared to inverse microemulsions resulted in narrow cluster size distributions.

Physicists have generally taken a different approach to cluster synthesis, based upon their expertise in high vacuum, molecular beam techniques combined with the use of mass spectrometers for mass selection and analysis. An excellent study of the cluster size distribution resulting from this synthetic approach is illustrated by the work of de Heer and coworkers.[3] They utilized a supersonic expansion of an atomic cluster source into a vacuum in the presence of an inert gas to create cluster beams.[3] They, and Brack *et al*,[27] discovered, using a mass spectrometer, that certain masses of clusters were produced in relatively large abundance. These "magic" sizes corresponded to the closing of atomic shells, analogous to stable nuclear shells from nuclear chemistry[28] or the electronic shells which form the basis of chemical bonding and the

periodic table. The stability of especially abundant masses of alkali metal clusters were shown to be described by simple "jellium" models. As a result, their physical[29] and optical properties were thoroughly investigated. These investigations led to the discovery of enhanced magnetic moments in small clusters of Co, Fe and Ni compared to their bulk counterparts.[30]

Magic size stabilities were also observed in solution-based synthesis of semiconductors.[31–33] However, it is difficult to compare the size-dependent physical and chemical properties (*e.g.* absorbance, PL, magnetic behavior, melting point, chemical reactivity) of clusters prepared by beam methods to clusters prepared by solution techniques. The comparison is complicated by the very important role of the cluster interface with its surroundings, also known as the embedding media effect.[5] For example, experiments show that clusters in a vacuum have very different optoelectronic properties compared to those dissolved in a solvent and/or coordinated to a ligand. Clusters in solution require tightly binding ligands to prevent association or "clumping" and in order to be perfectly dispersed. Thus, very small inorganic nanoclusters (1–3 nm) cannot be understood without also considering their organic interface or shell. Even in a vacuum, a naked cluster has unsatisfied bonding at its surface. This probably also requires some sort of surface reconstruction to minimize its energy, and this phenomena is absent from even the most refined descriptions and theories of cluster structure. For example, there is considerable controversy among theorists regarding the actual equilibrium shape of a cluster for a given number of atoms.[34,35]

In this review we emphasize the important role of synthesis methods and advanced characterization tools for both feedback and understanding of the size-dependent optical, magnetic, and catalytic properties. We discuss both alloys and core/shell nanoparticles. Quasi-random mixtures of atoms or nanoalloys have quite distinct properties from clusters where the atoms are segregated into a core and shell region. We also discuss the magnetic and catalytic properties of nanoclusters. We review three types of chemical methods for the formation of metal nanoclusters, but do not review gas phase or high vacuum methods of cluster synthesis instead referring the reader to the appropriate references mentioned above.[3]

The first method described, inverse micelle synthesis, is useful for both transition and base metal clusters. As examples of this method and the resulting physical properties we discuss the optical properties of Au, Ag, core/shell, and nanosize alloys of these metals. To enable the synthesis of core/shell and nanoalloys of two or more metals new methods of synthesis allowing the deposition of atoms of one metal type onto nanocluster "seeds" of another are necessary. Accordingly, we review methods for heterogeneous growth of core/shell nanoalloys and the resulting optical and magnetic properties. To illustrate magnetic properties we focus on nanometals of Co, Fe and Ni and alloys. We show there are major differences in the optical and magnetic properties depending on whether a core/shell or nanoalloy is investigated.

A second method widely employed to synthesize metal clusters relies on the chemical reduction of metal salts in polar

organic solvents by alcohols. To control the cluster growth with this method a strongly binding ligand should be present during the reduction. This ligand may be a polymer or a surfactant. Examples discussed include catalytically active transition metals such as Pt and Pd. This method has been extended to more difficult-to-reduce metals such as Fe or Co using high boiling point alcohols and solvents. In this form it is sometimes called poly-ol reduction.

The final synthetic method reviewed is the organometallic decomposition approach which has been most fruitfully used to produce Co, Fe and Ni clusters.[36] This method also requires metal coordinating ligands such as long chain organic acids or amines be present during the decomposition to prevent run-away cluster growth. This approach is most useful for producing clusters larger than 3–4 nm, though specialized examples exist of polymer stabilized 1–3 nm size clusters formed by organometallic decomposition under a reducing atmosphere of hydrogen.[37–39]

The size-dependent physical properties of individual clusters are changed when we form arrays of these clusters. We review how such arrays may be formed by methods such as self-assembly and electrophoretic deposition. Analysis of the structure of such arrays and the physical properties are also reviewed.

Other reviews in the area of metal nanoclusters may provide the reader with a broader perspective in addition to this review. We refer the reader to the reviews by Bonnemann *et al*, Quinn *et al.* and Mendes *et al*.[40–42]

Nanocluster synthetic methods

Inverse micelle synthesis method

The inverse micelle synthesis technique has been described extensively in several papers[18,21,24,43] and a patent.[23] The key aspect of this method which distinguishes it from either liquid or gas atomic aggregation processes (*e.g.* high-T thermal decomposition of organometallics to be described later) is that the metal cluster growth is controlled by the micro-hetero-geneous environment of the droplet-like inverse micelles. An additional advantage is the inexpensive, ready availability of simple salts as atom sources for the growth process. Most metal organic sources of metals do not decompose in an acceptable temperature range for liquid phase synthesis and are toxic and expensive. In most liquid phase synthesis protocols, control of the final cluster size can be regulated by the concentration of metal salt precursors—higher con-centrations favoring larger final clusters. Most metal salts used in the inverse micelle method are only soluble at concentra-tions of 0.01 M to 0.1 M using surfactant concentrations of $\sim$5–10 wt% ($\sim$.2 M), so there are only about 1–4 precursor ions per micelle. As a result, growth to the final observed sizes of N = 10–10000 atoms must occur *via* micellar diffusion, micelle collision, temporary interface fusion, and atomic interchange. Unlike growth in continuous phases which often result in power-law or log normal cluster size-distributions, the opportunity for atomic exchange between clusters can result in thermodynamically favored structures and clusters with narrow size dispersion. A surprising observation is that this process of atomic exchange between clusters can result in a

narrowing of the size dispersion with sample age.[44] This unexpected result contradicts that found in larger colloidal growth where kinetic processes like Ostwald ripening broaden the size dispersion with age.[45–47]

Other synthetic parameters in addition to precursor salt concentration can be used to control the final cluster size. Examples include the kinetics of the reduction step, the binding strength of the surfactant to the growing metal cluster and the micelle interior volume. The micelle volume roughly determines the maximum size of the small atomic clusters which may interchange during the growth or aggregation step of the synthesis. This cluster growth rate is determined by the diffusion rate of the micelles which is $\sim$2 orders of magnitude slower than would occur for the metal atoms in a continuous liquid phase. Thus, structural adjustments to atomic positions during intercluster atomic exchange are more probable due to the slow growth kinetics. This may favor thermodynamic structures and size distributions over metastable, kinetically controlled cluster structures. The slow growth rate with facile atomic exchange between and within a cluster may also explain why the inverse micelle growth process produces nanocrystal-line, not disordered clusters, regardless of the melting point of the bulk metal. However, sometimes the nanostructure differs from the bulk[43] depending on the surfactant used to form the inverse micelle. Examples of this phenomenon will be briefly discussed for the case of Co, Fe and Sn cluster synthesis.

The use of inverse micelles as nanosize reactors has been refined significantly since our first description of metal nanocluster synthesis using inverse micelles in 1989.[48] The most significant change is the addition of strongly binding surfactants, such as thiols or amines to the inverse micelle solution containing the dissolved metal salts. These molecules bind to the cluster surface during or after the chemical reduction and cluster growth and alter the growth rate. In some cases it has been shown that addition of these molecules can initiate an etching process which leads to a narrowing of the cluster size dispersion with time.[44,49–52]

The addition of strongly binding molecules like alkyl thiols allows the application of liquid chromatographic analysis of the nanocluster size and size dispersion.[52] Using this method it has been discovered that when thiols are added prior to chemical reduction, they can significantly alter the final nanocluster size resulting in smaller, less polydisperse clusters. This is reasonable since the thiol–metal bond is stronger and thus inhibits the cluster growth more strongly than most nonionic and cationic surfactants used to form inverse micelles. The thiols, though present in much lesser amounts than the surfactants used to form the inverse micelles, compete very effectively for binding sites on the growing nanocluster surface. Due to their strong binding properties thiol passivat-ing agents also permit purification and removal of ionic by-products and most of the surfactant micelles used to solubilize the metal salt precursors. The stabilization of the nanocluster surface by a strongly binding ligand is critical to the variety of purification approaches described in the literature.[51,52]

Many papers describing Au nanocluster synthesis use phase transfer catalysts which are usually long chain alkyl quatern-ary ammonium salt surfactants.[51,53] However, there are some misconceptions about the role of the cationic surfactants used

in this synthetic approach. First, the typical recipe requires water to initially dissolve the salt, (typically $HAuCl_4$ or $NaAuCl_4$), and then requires this aqueous salt solution to be brought into contact with an immiscible toluene solution containing a cationic surfactant, (usually tetraoctylammonium bromide, (TOAB)). It is important to ask why only certain quaternary ammonium surfactants will actually solubilize the gold salt into the organic phase? The reason is that very hydrophobic, long-alkyl chain surfactants are required to ensure both the formation of spherical micelles in the organic (toluene) phase and the total exclusion of water from that phase. We discovered several years ago by neutron scattering (unpublished work), cationic, quaternary ammonium surfactants spontaneously form inverse micelles in toluene. Thus, they are able to directly solubilize a wide variety of metal salts without the use of water. This observation was first described by our group using didodecyldimethyl ammonium bromide (DDAB) in toluene.[23,24] It is also possible to use linear alkane solvents with these surfactants, but geometric considerations in the tail group packing often require a co-surfactant like hexanol be added to "fill in the gaps" in the micellar surfactant droplet interface with linear alkanes.

Since these cationic surfactants act as a micelle-forming agent capable of directly solubilizing a variety of metal salts, water does not need to be introduced into the system. This allows for the use of strong reducing agents such as $LiBH_4$ in tetrahydrofuran (THF), or $LiAlH_4$ in THF or toluene. Generally, these reducing agents are superior to $NaBH_4$ in water which is typically used to produce Au clusters by reduction of $HAuCl_4$ in two phase systems. $NaBH_4$ in neutral aqueous solution is unstable with respect to hydrolysis. However, if $NaBH_4$ is the reductant of choice, only highly alkaline solutions (~ 4 NaOH:$NaBH_4$) should be used to effect reductions. These caustic reducing solutions are quite stable and are actually sold by Aldrich as stock ~ 4.4 M $NaBH_4$ in ~ 14 M NaOH solutions. They can be diluted into water, as desired.

In the case of gold or silver, the precursor metal salts are so easily reduced that the use of alkaline $NaBH_4$ in water as we described in our early work is quite acceptable. However, this reducing agent is not as effective for the reduction of Pt or Pd salts, and is completely ineffective for formation of metallic Fe, Ni, Co, Si, or Ge. In the case of Fe, Ni or Co, the corresponding metal boride will form.

Cluster formation in polar organics by chemical reduction in the presence of stabilizers

The synthesis of ligand stabilized metal nanoparticles using an aqueous alcohol reduction of a metal salt was first reported by Hirai et al.[54] This method of metal cluster formation utilizes chemical reduction of an organic soluble metal-salt precursor. Either a coordinating or non-coordinating solvent can be used, or some combination thereof. Hirai also investigated both the catalytic activity and the formation mechanism of the metal nanoparticles protected by the polymers poly(vinyl alcohol) or poly(N-vinyl-2-pyrrolidone) (PVP). The synthesis and catalytic activity of PVP-stabilized metal nanoparticles was also studied by Bradley et al.[55] They established a synthetic method to form PVP-protected Pd nanoparticles by the water-free reduction of Pd acetate using an alcohol.

In later work, a surface-active, (but not micelle forming), species like dodecanthiol, C12SH, or tri-octylphosphine, TOP, was added to prevent run-away growth during the chemical reduction. This approach is best described in the excellent review by Schmid,[13] and exemplified by the reaction which produces Au($N = 55$) clusters.

Bradley et al. developed a method for producing bi-metallic clusters of palladium–copper by a high temperature reduction in an alcohol.[56] The reported particle size was 3–5 nm as determined by TEM. Energy dispersive X-ray spectroscopy, EDAXS, of the clusters was used to show individual particles were bimetallic. However, as in all analysis using TEM, only certain sections of the grid were analyzed, so size or compositional segregation, which is now known to be common, does not rule out the presence of significant populations of either larger or smaller particles with different compositions from that reported.

Chaudret et al. also discovered a versatile method for metal cluster formation using reduction of metal organics with hydrogen gas.[37] The advantage of this method is that the ligands in the metal organic complex could be reduced and expelled from the nanocrystal surface and thus were less likely to contaminate the cluster surface. In order to control the size, the polymer PVP, just as used in the original work of Hirai, was employed as a stabilizer for Co clusters. Some cluster size control was provided by formation at three different reaction temperatures.[36] The quality of the small, ~ 1.6 nm clusters was demonstrated by magnetic measurements where the magnetic moment per atom exceeded that of the bulk material by about 10%. This is a remarkable result as we discuss in more detail later in this review in the context of magnetic properties. Normally, surface ligands and defects quench the magnetic response of small clusters. A similar enhancement of the magnetic response of alloy nanoparticles of ~ 2 nm CoRh and CoRu was reported in later work by the same group.[57]

It is possible to use other types of reducing gasses to form metal clusters as demonstrated by Rodriguez and co-workers using CO as the reductant to produce Pt clusters.[58] In this work the importance of the ligand used to prevent cluster–cluster aggregation in the final nanocrystalline structure was demonstrated. A restructuring of the originally isolated colloids by the addition of tri-phenyl phosphine was reported. The small, 1–2 nm Pt nanoclusters formed an icosahedral structure when this ligand was added. For small clusters, the high surface mobility and large numbers of surface atoms, makes such ligand induced structural changes facile. In fact, later work on 1.8 nm Fe showed that a similar ligand controlled nanostructure was observed.[38] As in the case of the Co work by the same group, magnetic measurements shows an enhanced high field magnetic response indicative of a clean cluster surface where the ligands do not quench the magnetic moment. Wilcoxon et al. first demonstrated cluster nanostructure control by surfactants in larger nanosize Fe clusters where both α and β phases of iron were produced.[43]

In later work Ely et al. extended the ligand-stabilization approach to Ni nanoclusters, again using PVP as a stabilizer and hydrogen gas as a reductant.[59] The use of hydrogen as a

This journal is © The Royal Society of Chemistry 2006

Chem. Soc. Rev., 2006, **35**, 1162–1194 | 1167

reductant under ambient temperature conditions was shown by the same group to be useful for formation of Ru nanoclusters.[60] The claim was that these 1.1 nm nanoclusters had an hcp structure is difficult to believe given that fact that such clusters only contain ∼13–20 atoms and so would not have enough translational symmetry to diffract X-rays or electrons and thus identify the structure. These clusters consist mainly of surface atoms (>80–90%) and the structure of the cluster surface cannot be determined by diffraction methods.

In their work, the Chaudret group demonstrated that the choice of stabilizer had a significant impact on the dispersion of the clusters. Amines and thiols, for example, resulted in aggregation of the clusters. Wostek-Wojciechowski et al. provide a review of this general method of hydrogen reduction for the case of Co, Ru and Rh.[61] The claim was made that the atomic surfaces of these ∼2 nm clusters were all zero-valent, but it wasn't clear this was true for individual clusters since the measurement was an ensemble average measurement as is very common. To identify the composition and oxidation state of subpopulations of clusters requires chemical separation by techniques such as liquid chromatography followed by sample collection and analysis of the composition.

Another review by Chaudret summarizes the synthesis and properties of clusters formed via organometallic decomposition under hydrogen and the important role the stabilizer ligand plays in the nanostructure of the cluster.[37] The weakness of the claims of ligand induced nanostructural changes in this review is due to the small size, 1–2 nm, of the clusters produced by this approach. The small numbers of atoms per cluster make application of diffraction methods of structural determination quite difficult. The fact that clusters with sizes of around 1.1, 1.6 and 1.9 nm were so often observed by the Chaudret group argues for a thermodynamic size control in their method since, as we discuss later, these sizes are close to closed shells of 13, 55 and 147 atoms in each cluster. This may also explain the narrow size dispersion and excellent magnetic properties reported.

Two refined examples of cluster synthesis based upon chemical reduction in continuous solution in the presence of polymeric stabilizers method are embodied in the work by Teranishi et al. for production of Pt[62] or Pd[63] clusters. We choose to examine these two studies in more detail because they embody most of the key chemistry found in continuous phase chemical reduction to form clusters in solution. Teranishi and co-workers found that the mean diameter of monodispersed Pd nanoparticles could be controlled from 17 to 30 Å in a one-step chemical reduction of an ionic Pd salt by changing the amount of protective polymer, poly(N-vinyl-2-pyrrolidone) (PVP) and the kind and/or the concentration of alcohol in the mixed water–alcohol solvent used to dissolve the metal salt precursor. Although increasing the amount of protective polymer made the size of Pd nanoparticles smaller, the particle size appeared to have a lower limit determined by the kind of alcohol. On the other hand, monodispersed Pd nanoparticles of smaller diameter were obtained in the order methanol > ethanol > 1-propanol, indicating that a faster reduction rate of $[PdCl_4]^{2-}$ ions is an important factor to produce smaller particles. In the work of Teranishi et al., the alcohol acts as a reducing agent and their observed dependence of size on alcohol type indicates that shorter chain alcohols act as stronger reductants. Once the monodispersed Pd nanoparticles were obtained, the larger particles with a narrow size distribution could be synthesized by using a stepwise growth reaction. The heterogeneous deposition of atoms onto preexisting cluster "seeds" is described more completely below for the case of Au and Ag.

It is worth noting that in the inverse micelle approach, faster reduction using stronger reductants also produces smaller particles. However, the range of $[PdCl_4]$ that can be used in continuous solution is nearly one order of magnitude smaller than employed in the inverse micelle approach since concentrations above ∼1 mM increase the cluster size polydispersity significantly. So, smaller numbers of clusters can be generated in a given reaction volume. A more limited range of particle size is also obtained since larger salt precursor concentrations are precluded. Also worth noting is that certain preferred sizes in the range reported by Teranishi et al. correspond to the sizes expected for the especially stable clusters observed by Schmid.

It is interesting that the polymer PVP is so widely used as a ligand for controlled growth of metal clusters. We speculate that this is due to its ability to ligate to the metal surface from both its adjacent nitrogen and oxygen atoms. The bidentate nature of this ligation seems especially important as the metal cluster size increases. In fact, we find polymeric stabilizers to provide superior steric stabilization relative to monodentate ligands such as thiols and primary amines for cluster sizes greater than around 8 nm.

The Pd nanoparticles obtained in the above synthesis had fcc structures like that of bulk Pd, although the lattice constant increased with a decrease in the particle size. Interestingly, the same synthesis using PVP as a stabilizer for Pt clusters[62] did not show any change in lattice constant with decreasing size, though Pt also has an fcc structure in the bulk. Teranishi and co-workers also demonstrated an electrophoretic deposition technique to form layers of Pt nanoparticles on a substrate. Unfortunately, there are major defects in the monolayer films in their TEMs. We return to the topic of the formations of arrays of clusters on substrates later in this review.

In order to reduce metals like Co or Fe with alcohols a higher reaction temperature is required. This requirement influenced the development of poly-ol reduction using glycols dissolved in high boiling point ethers.[9,64] In many cases a glycol with a long chain could be used and this molecule was found to act as both stabilizer and reductant. The size distribution of the Fe particles formed by this approach is not as narrow as can be achieved with successive heterogeneous growth stages starting from smaller, more monodisperse seeds.[64] It is also not as simple to prepare clusters with sizes less than 3 nm.

In all the formation methods for transition and base metal clusters the general principle of the use of smaller amounts of stabilizing ligand and larger precursor metal salt concentrations to form larger clusters is valid. However, one generally observes a substantial increase in cluster size distribution when clusters larger than 5 nm are formed. This observation may originate from the common use of small organic chain length amines or alcohols (e.g. oleic alcohol or oleyl amine) as stabilizers. The steric stabilization provided by this type of

ligand is usually inadequate for larger clusters which require a higher molecular weight ligand such as PVP. The earliest syntheses of Co, Ni and Fe clusters by thermolysis of organometallic precursors employed such ligands as described in our introduction and elaborated in the next topic.

Organometallic decomposition in the presence of stabilizers

Decomposition of a thermally labile, oil soluble, metal-organic precursor is the oldest approach for non-aqueous synthesis of metal nanoclusters. This approach requires the presence of a surfactant-like stabilizer, such as a block co-polymer.[6] Fairly monodisperse colloids can result under the proper conditions. This method is typically only used for base-metal nanocluster synthesis like Co, Fe, Ni since an available thermally unstable metallo-organic is required such as $Fe(CO)_5$, $Co_2(CO)_8$, $Ni(CO)_4$. These compounds are very air-sensitive and either mildly or severely toxic. It is thus important that all handling be done in either a glove box, or by Schlenk-line methods. Due to the rapid growth rate compared to chemical reduction methods, the final clusters are usually highly defective and require significant annealing at elevated temperatures to produce high quality samples. The final material properties, (*e.g.* saturated magnetic response) are thus typically only a small fraction of that found in the corresponding bulk materials.[6–8]

Metal nanoclusters can also be synthesized in solution through high-T reduction of organometallic precursors by glycols in coordinating solvents like diphenyl ether. Murray *et al.*[9] have recently refined this "poly-ol" method to produce base metal clusters of a variety of sizes of Co, Fe, and Ni. Empirically chosen surfactants are typically used to stabilize the growth of metal nanoclusters. In this method the nanocluster size is increased by increasing the amount of precursor and/or decreasing the amount of surfactant. There is a significant amount of trial and error in the selection of the surfactant. Sometimes, more than one stabilizer may be employed—a common combination being a primary amine and a long-chain organic acid. A drawback of this method is the formation of unwanted metallic films and/or incomplete reduction so the yield is not 100%. Also, this method requires high boiling point solvents since the reduction typically takes place at temperatures between 200 °C and 300 °C. In order to achieve an optimal synthesis using this technique, some empirical variation of temperature and reducing agent is necessary. This is because some of the solvents may not allow solubilization of all the available components (metal-organic, poly-ol, stabilizer *etc.*).

In some cases, this method yields nanostructures not commonly found in the bulk phase. For example, Murray and co-workers discovered an ε-Co phase when employing this method to make nanosize Co.[9] This nanophase could be transformed to the normal hcp Co upon heating. Unfortunately, the ε-Co phase has very poor magnetic response compared to hcp phases. The heating can lead to sintering between particles and loss of nanostructure, so this synthetic approach for Co is less favorable than other methods. A similar failure to achieve the highly anisotropic, normal FePt phase occurs when using this method to form a nanoalloy of FePt, and a method of forming the desired phase is currently being pursued by several groups.[10,64]

Nanosize alloys can also be made by this approach with a high degree of nanocrystalline perfection. A very good example of the variables controlling cluster size in such nanoalloys was given by Shevchenko and co-workers.[39] $CoPt_3$ nanocrystals were synthesized by organometallic decomposition of the precursors $Co_2(CO)_8$ and Pt(acetoacetonate)$_2$ = Pt(Ac)$_2$ in the presence of a bulky organic carboxylic acid, adamantane carboxylic acid (ACA) and a glycol reductant. By controlling the reaction temperature, concentration of the ligands, and even the precursor ratio, the final cluster size could be controlled between 3 and 18 nm, much larger than the range typically achieved in organometallic based cluster synthesis. In contrast to the observation of a decrease in the cluster size with increasing stabilizing agent found in inverse micelle synthesis at room T, increasing the ACA stabilizer concentration in this synthesis always resulted in larger size clusters, regardless of reaction T.

The Weller group correctly, we believe, based upon our group's experience with synthesis of metals from metal organics, asserted that the presence of stabilizing ligands such as ACA effects a reaction at elevated temperatures in which the ligands originally bound to the metal (*e.g.* CO in the case of Co and Ac in the case of Pt) are displaced by the surfactant, ACA.[39] This produces a more or less labile metal-organic species with respect to decomposition. The evidence for this assertion was the lack of reaction of $Co_2(CO)_8$ to produce Co clusters in the absence of ACA. A similar failure to produce anything other than bulk Pt metal was found when the Co precursor and ACA were omitted. The reaction only produced high quality clusters in the presence of both precursors and ACA. An analogous situation occurs in the decomposition of dimethyl cadmium to form CdSe clusters in the presence of triocylphosphine, TOP. TOP complexes with the Cd(II) from which the decomposition then proceeds. A similar mechanism likely controls the synthesis when CdO is used in place of dimethyl cadmium.[65]

The Weller group (Shevchenko *et al.*) observation of the importance of ligand substitution to the successful formation of $CoPt_3$ clusters illustrates a very general process in cluster synthesis in the presence of surfactant ligands.[39] A metal salt is dissolved in a surfactant system and the original ligand or counterion for the metal is replaced leaving the metal partially or fully coordinated to the surfactant. This occurs when dissolving metal salts in inverse micelles as demonstrated by a color change upon ligand replacement. This can be quantified by an alteration of the optical absorption caused by charge transfer bands as monitored using UV-Visible spectroscopy. For example, in the synthesis of Au clusters using a cationic surfactant with a bromide counterion, first described by our group in 1993, the chloride ligand in the complex gold salt, $HAuCl_4$ which, when dissolved produces a yellow colored solution in either water or with a cationic surfactant with a chloride counterion, results in a orange red inverse micelle solution in toluene because of exchange of the Br for the Cl in the Au complex.[24] Not surprisingly, dissolving $HAuBr_4$ in the same solutions results in the identical orange red solution with identical absorption characteristics. This complexing process

can be extended further upon addition of significant amounts of an alkiol thiol which causes the orange red solution to become clear as the thiol replaces the Br in the ligand sphere of the Au salt.[49]

In the $CoPt_3$ study by the Weller group[39] it was reported that the Co : Pt precursor ratio had no effect on the final composition of the clusters which was always $CoPt_3$. By contrast, in a study of nanocluster, FePt alloy formation, the ratio of the precursors strongly influenced the final cluster composition.[64] Another surprising observation was the fact that the reaction was always run with a stoichiometric deficiency in Pt, yet no Co clusters were formed. However, larger ratios of Co : Pt did result in smaller $CoPt_3$ clusters at a fixed reaction T. It was argued that larger amounts of the Co_2CO_8 precursor caused increased amounts of nucleation since it was assumed that the formation of small, pure Co clusters was the first step in the reduction of the $Pt(Ac)_2$ precursor. With more nuclei and the fixed amount of precursor, the final cluster size should be smaller.

The size dispersion of the $CoPt_3$ clusters appeared to be low based upon small angle X-ray (SAXS) data in which several minima in the structure factor were observed.[39] This observation and the SAXS size were consistent with their TEM size analysis which is more subjective since only limited numbers of nanoparticles can be analyzed. SAXS, being a true ensemble average measurement, gives a better statistical measure of average size and size dispersion. However, if the cluster size is too small, (e.g. <4 nm), SAXS also suffers some practical limitations to be discussed.

Despite the excellent lattice fringe images with very few defects the magnetic saturation values for $CoPt_3$ clusters were quite low compared to bulk material, ranging from 2 emu g^{-1} for 3.8 nm clusters to ~10 emu g^{-1} for 9.4 nm clusters. Though an explanation for the low magnetic response was not given, possible surface defects or oxidized sites will reduce the magnetic moment. Low magnetic response is commonly observed in pure Co and Fe clusters synthesized using organometallic decomposition in the presence of oleic acid and oleylamine and, in this case, it is known that an oxide layer at the surface may be responsible. It is likely that a metal oxide surface is required to effectively bind to organic carboxylic acid stabilizers since we have found long chain organic acids are ineffective stabilizers for Co, Ni and Fe clusters made by hydride reduction where the metal cluster surface is not oxidized. The fact that Shevchenko et al[39] found ACA to be very effective in stabilizing their $CoPt_3$ nanoclusters implies the cluster surface may have been partially oxidized, perhaps explaining the low magnetic response despite the absence of internal cluster defects.

One of the most useful aspects of the study of $CoPt_3$ clusters was the identification of the nucleation rate as controlling the final cluster size. A good rationalization of the role of T, stabilizer concentration, and Co : Pt ratio effects on the final cluster size was provided. An open question was why $CoPt_3$ was always observed despite a wide range of Co : Pt precursor ratios investigated. Presumably the excess Co reacted to form Co clusters once the Pt precursor was consumed. However, they noted that in the absence of the $Pt(Ac)_2$ precursor, the Co_2CO_8 precursor did not decompose in the range of temperatures investigated. So the $Pt(Ac)_2$ precursor must be crucial in initiating the Co precursor decomposition. We have observed a similar situation in the co-reduction of Au and Ag salt precursors where the presence of the Au precursor increases the ease of reduction of the Ag. So, sometimes alloy nanoparticles can be more easily synthesized than clusters of their individual components.

Nanocluster characterization

Synthesis optimization through characterization feedback

For optimization of nanocluster synthesis methods rapid, quantitative feedback concerning final cluster size, shape, optical properties and their relationship to the myriad synthetic variables is necessary. It is well known that advances in organic synthesis have been facilitated greatly by the advent of modern analysis methods, such as Fourier transform infrared spectroscopy (FTIR), gas chromatography/mass spectrometry (GC/MS), liquid chromatography, (LC) using photodiode array absorbance measurements, (LC/PDA), nuclear magnetic resonance (NMR), etc. Without such feedback, the synthetic chemist is ignorant with respect to whether changes in synthetic protocol are improving the final product. Unfortunately, extending such analytic methods to the analysis of surfactant-stabilized inorganic nanoclusters is not straightforward and so only limited feedback is available to guide the development of the synthesis process. The development of refined synthesis protocols for nanoclusters—examples being transition metal nanoclusters as shown by our group,[23] and II–VI semi-conductors (mainly CdSe) as shown by Murray, Norris, Peng and Dabbousi[66–69]—have benefited from the size-dependent optical properties of the clusters apparent to the human eye which can be quantified by simple absorbance measurements.

For example, solutions of Au and Ag clusters have clearly identifiable, size-dependent visible colors (absorbance) which allow rapid feedback as to size and polydispersity using simple absorbance spectroscopy. They are also relatively air-stable which accounts for the numerous studies in the literature. In the case of nanosize Au or Ag, one can perceive, even with the naked eye, color changes corresponding to ~2–4 Å in size, and using an absorbance spectrometer, 1–2 Å size differences.

Since the optical properties of clusters of Au, Ag, and nanoalloys are sensitive to size, shape, and composition, monitoring the absorbance of size or shape selected clusters provides useful feedback concerning the success of a given synthesis. Similarly, magnetic response measurements on clusters of Co, Fe and Ni are very sensitive to average size, structure, and size dispersion and can yield useful information regarding their synthesis. However, to monitor cluster size dispersion requires a size-separation technique. In this section we describe size-exclusion chromatography (SEC) which can be very useful for this purpose. We first discuss more traditional characterization techniques such as TEM as applied to nanoclusters then briefly discuss scattering techniques such as dynamic light scattering (DLS) and small-angle X-ray scattering (SAXS). Other structural and composition techniques such as selected area electron diffraction (SAD) and

X-ray diffraction (XRD) and X-ray fluorescence (XRF) applied to clusters will also be reviewed briefly.

Transmission electron microscopy (TEM, HRTEM)

Accurately characterizing the physical and chemical properties of nanoclusters presents a formidable challenge and requires correlation between several types of characterization techniques. This was noted previously by Brus who recognized the limits of the most commonly used cluster characterization tool, transmission electron microscopy (TEM), as lacking sensitivity to possible nanocluster surface reconstruction.[31] In addition, for small metal clusters, for example Ag, beam heating or cluster melting effects can occur during imaging, which obfuscates the boundary between cluster and grid and results in cluster sintering or fusion. TEM is also not completely accurate in determining the actual size of the cluster since the size is usually uncertain to at least one or two lattice fringes, typically around 2 Å. TEM reveals mainly the internal structure of a cluster, so surface structural information is lacking. Finally, when a polydisperse population of clusters is deposited on a TEM grid larger clusters tend to segregate into regions which exclude the smaller clusters, giving the impression of a narrower size dispersion than is the real case.[70]

High resolution TEM (HRTEM) is useful for determining metal core (D_c) sizes to an uncertainty of one lattice constant (± 2 Å) core. However, in the size range of $D_c \sim 2$ nm this measurement uncertainty is still large even assuming a perfectly monodisperse sample with all the clusters in an identical focal plane on the holey carbon grid and identical nanocrystal orientation.

Nanocrystal orientation is very important for small crystals. For example, if a randomly oriented region of monodisperse icosohedral Au crystals is examined with $d<111> = 2.1$ nm and $d<100> = 2.7$ nm, one obtains the number average D_c(TEM) $\sim 2.4 \pm .3$ nm, but this is not due to size dispersity.

In general, determining the size dispersity of a sample is difficult and tedious with TEM alone since the area viewed is such a small part of the entire sample. Optical measurements such as absorption lend more insight into the ensemble average properties of the system, but it is still difficult to differentiate surface and quantum size effects, both of which scale with $1/r$ (r = cluster radius).

High pressure liquid chromatography (HPLC) and size exclusion chromatography (SEC)

In order to overcome the above mentioned difficulties, attempts to determine the size distribution of nanoclusters and separate different size fractions were undertaken by Fischer *et al.* for CdS[32] and later by Brus *et al.* for Si[71,72] and Wilcoxon *et al.* for metal and semiconductor clusters.[73] These groups used high pressure liquid chromatography (HPLC) or size exclusion chromatography (SEC, a type of HPLC) to separate the different populations of clusters in their solution samples. Fig. 2 shows some of the first HPLC performed on Si nanoclusters.[72] The width of the chromatographic peak allows determination of the size distribution in the sample being analyzed. The time at which the peak elutes permits calculation of the average size of the population being
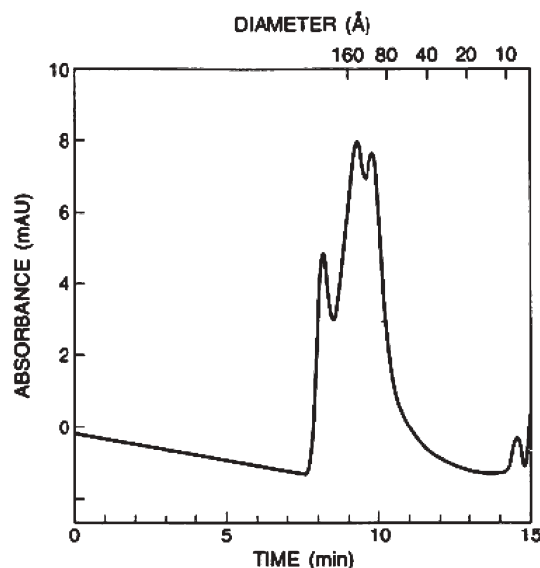

Fig. 2 HPLC of Si nanoclusters showing a fairly large size distribution. (Reprinted with permission from reference 72: K. A. Littau, P. J. Szajowski, A. J. Muller, A. R. Kortan and L. E. Brus, A luminescent silicon nanocrystal colloid via a high-temperature aerosol reaction, *J. Phys. Chem.*, 1993, **97**(6), 1224–1230. Copyright 1993 American Chemical Society.)

analyzed if specific chemical interactions between the column and cluster can be ignored. Columns are calibrated using nearly monodisperse standards of known hydrodynamic size. As can be seen from Fig. 2, the size distributions varied for each case and seemed to depend upon the synthesis technique utilized.

Although some of the early data using HPLC for cluster analysis showed a broad cluster size distribution, the feedback this technique provides is still valuable for synthesis optimization. HPLC provides information concerning the ensemble, or total cluster population, average (number average) hydrodynamic sizes present in a cluster sample. In contrast, TEM measures only the high contrast inorganic core. As synthesis techniques for metal nanoclusters evolved and were refined, the potential for understanding size and surface related properties of nanoclusters became evident. For the reasons mentioned above size determination by high resolution SEC, complemented by HRTEM, has major advantages. Fig. 3 shows a HRTEM of Au, $D_c = 1.8$ nm particles which shows the atomic lattice fringes from this HPLC purified sample and illustrates the effects of crystallographic orientation and focal plane effects on the apparent cross-sectional diameter of this nearly monodisperse sample.[52] A chromatogram showing the separation $D_c = 2$ nm Au nanoclusters (D_c = inorganic core diameter) from the solvents and surfactants used to produce them is illustrated in Fig. 4.[52]

With HPLC, not only can hydrodynamic size and polydispersity be monitored but the concentration of clusters or chemicals of a given size can also be determined by the relative areas under the elation peak *vs* known standards. By combining HPLC–SEC with other characterization methods such as TEM, or dynamic light scattering (DLS), which can also determine hydrodynamic size and extent of polydispersity,
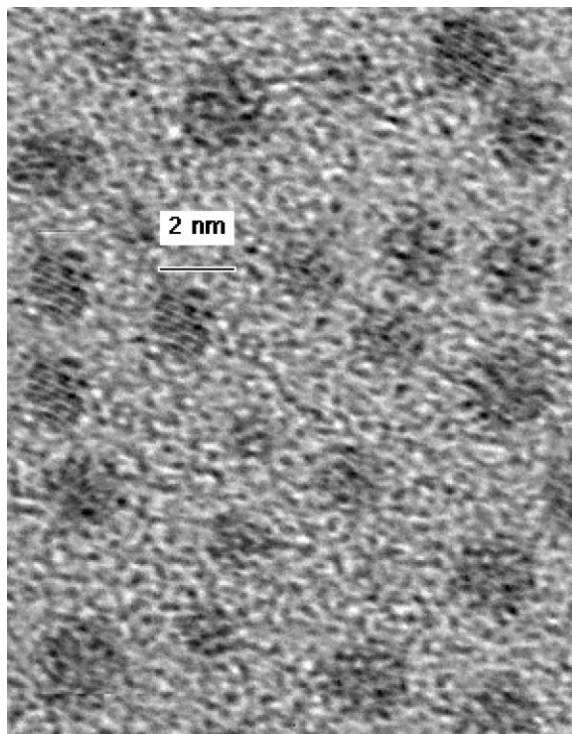
Fig. 3 High resolution TEM (HRTEM) of a field of 1.8 nm clusters. The atomic lattice fringes and facets of the nanoclusters can be observed in the image. (Reprinted with permission from reference 52: J. P. Wilcoxon *et al.*, Size distributions of gold nanoclusters studied by liquid chromatography, *Langmuir*, 2000, **16**(25), 9912–9920. Copyright 2000, American Chemical Society.)
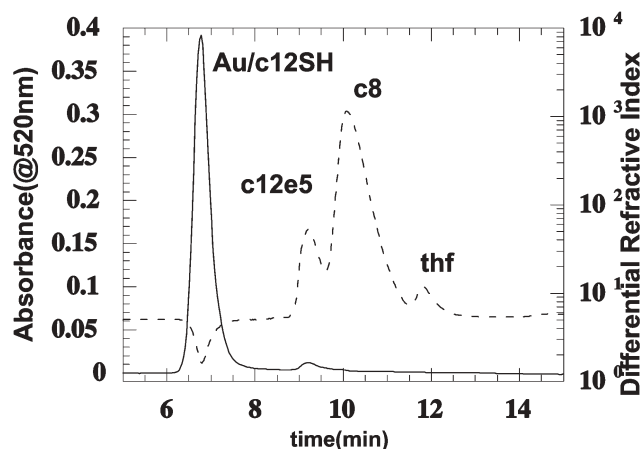

Fig. 4 Absorbance at 520 nm and refractive index detector response *vs* chemical elution time for Au clusters (solid curve), and other chemicals (dashed curve). The other chemicals are a nonionic surfactant (C12E5), octane (C8), and tetrahydrofuran (THF). The smaller chemicals were separated from the larger dodecanethiol, C12SH, stabilized Au clusters by a 250 mm × 7.8 mm, 500 Å pore size polystrene 10 mm microbead column and a mobile phase of toluene. (Reprinted with permission from reference 52: J. P. Wilcoxon *et al.*, Size distributions of gold nanoclusters studied by liquid chromatography. *Langmuir*, 2000, **16**(25), 9912–9920. Copyright 2000, American Chemical Society.)

(min)) for the PL1000 (Polymer Laboratories, 1000 Å) column used in that reference, D_h was obtained for each fixed size core + shell. This relation was valid for 1 nm < D_h < 10 nm Columns are available with larger pore sizes which extend this range to larger values. For further information the reader

and optical absorbance measurements, a more complete "picture" emerges combining information about both size and surface chemistry. For example, the elution time (t_e) for a properly passivated Au nanocluster sample with a hydrodynamic diameter (D_h) obeys the relation, log $D_h \sim t_e$, allowing one to obtain a metal core diameter after subtraction of the thickness of the organic passivating layer.[52] This thickness can be determined by taking a sample with a single core size as determined by TEM and adding a series of alkyl thiols, designated herein as C_kSH, with chain lengths k of 6 < k < 16, to the toluene mobile phase and obtaining D_h from the shell thickness and subtracting the known TEM core size. Fig. 5 shows an example of the size separation capability of SEC for a single core size, D_c = 2.0 nm and three shell thicknesses with alkyl chain lengths of k = 6, 10, and 14.[52] This figure illustrates that clusters with different total hydrodynamic sizes due to organic shell differences may be separated using SEC. The relative areas under the peaks in Fig. 5 also reveal that longer chain alkyl thiols "stick" to the cluster surface more effectively than shorter ones since the elution peak area increases systematically with chain length.

The organic passivating shell thicknesses obtained by SEC using the known core size and the retention times shown in Fig. 5 agree well with values calculated from known C–C bond lengths in linear alkanes and confirmed by SEC. Using the best fit to a series of linear alkanes and polysytrene polymer standards we established D_h (nm) = 608*exp(−.62525*t_e
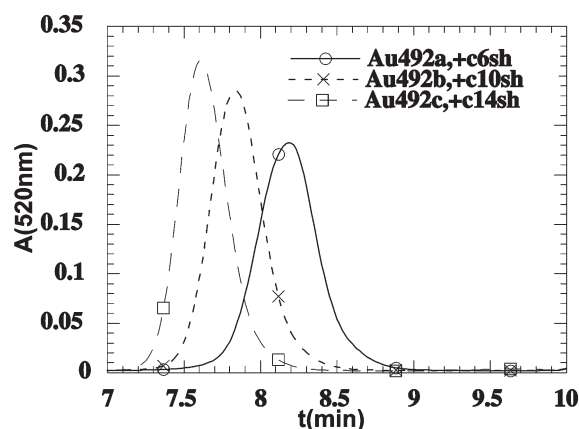

Fig. 5 Effect of chain length on the hydrodynamic diameter of Au nanoclusters stabilized with shells of alkyl thiols. An HPLC chromatogram of absorbance at 520 nm A(520 nm) *vs* elution time shows elution peaks which depend on the thiol shell thickness for a fixed Au nanocluster core size. The alkyl thiols, CkSH, k = 6,10,14 were added after reduction. The SEC column used was a Polymer Labs 1000 Å column and the mobile phase was toluene at 1 ml min^{-1} flow rate. (Reprinted with permission from reference 52: J. P. Wilcoxon *et al.*, Size distributions of gold nanoclusters studied by liquid chromatography, *Langmuir*, 2000,**16**(25), 9912–9920. Copyright 2000, American Chemical Society.)
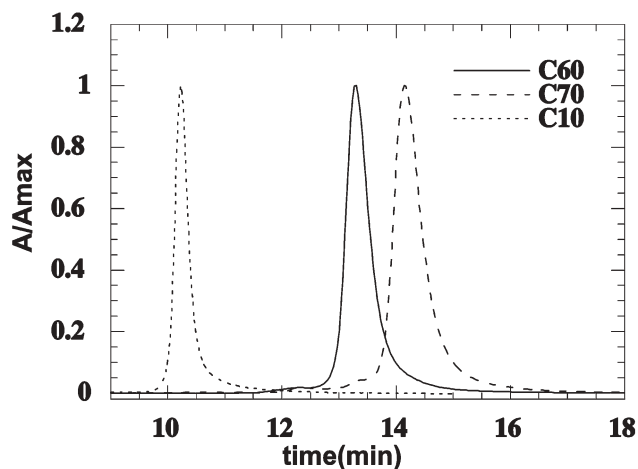
Fig. 6 Normalized absorbance, A/A_{max} vs elution time showing the instrumental linewidth for samples of decane (C10), buckyballs, C60, and C70 run on a 500 Å polystyrene column in toluene. (Reprinted with permission from reference 52: J. P. Wilcoxon *et al.*, Size distributions of gold nanoclusters studied by liquid chromatography, *Langmuir*, 2000, **16**(25), 9912–9920. Copyright 2000, American Chemical Society.)

Fig. 7 Normalized absorbance at 520 nm, A/A_{max} vs elution time demonstrating that the size distribution of Au clusters can be as narrow as buckyballs, C60 The C60 elution time has been time shifted to overlap that of the Au nanoclusters for comparison. (Reprinted with permission from reference 52: J. P. Wilcoxon *et al.*, Size distributions of gold nanoclusters studied by liquid chromatography, *Langmuir*, 2000, **16**(25), 9912–9920. Copyright 2000, American Chemical Society.)

should consult the HPLC reference book by Yau, Kirkland, and Bly on this subject.[74]

For other nanoclusters such as Si, Ge, Co, Ni, Fe the best mobile phase choices appear to be tetrahydrofuran, THF, or acetonitrile, ACN. With careful optimization of an SEC system the retention time (*i.e.* D_h) of high quality, stable nanocluster samples can be reproduced to within the instrument resolution of 0.01–0.02 minute over periods of greater than 1 year. This corresponds to a size resolution of ~ 1 Å. Along with size information, shape differences in cluster subpopulations influence the retention time. Near baseline separation of buckmasterfullerene, C60 from C70 on a typical PL500 column can be achieved, even though these fullerenes differ in hydrodynamic size by only ~ 1 Å. This separation is demonstrated in Fig. 6.[52]

The chemistry of the cluster surface can also be studied by using specific column chemical functionalities.[73] In this approach, columns with functional groups similar to that expected of a substrate molecule are used and the degree of interaction or chemical affinity between the cluster surface and column gives a measure of the binding strength. Long retention or elution times correspond to strong bonding. Thus, metal oxide cluster surfaces can be distinguished from metal clusters of the same size and shape.

Unlike reverse phase chromatography columns, for SEC columns the instrumental elution peak band-broadening does not depend on elution time, but simply on the average size of the microgel particles used to pack the column. For example, the high resolution columns used in previous studies were packed with porous 5 μm particles and had significantly narrower inherent band-broadening than less expensive columns packed with 10 μm particles of the same material. This column band-broadening is determined experimentally by using a known monodisperse sample and the same column used for study of the unknown samples. Using decane (C10) as
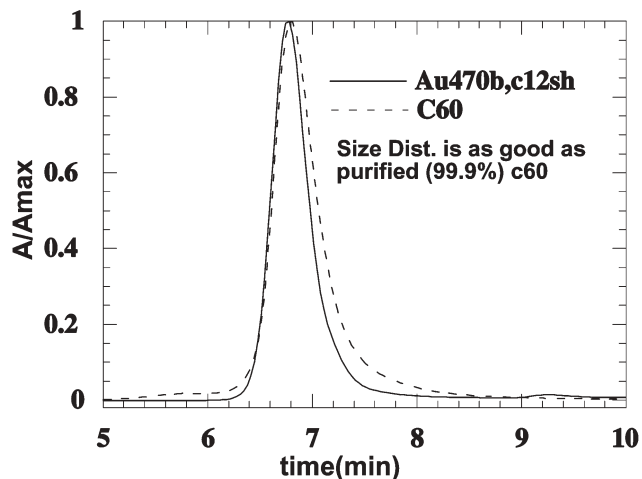
the known sample, we found the full width at half max for the elution time ($\Delta t_{1/2}$) is 0.25–0.27 min whereas this quantity for purified buckyballs (C60 and C70) is 0.40 min. From shape considerations the C60 standard seems more appropriate to compare to our spherical nanocluster samples. Cluster elution peaks whose temporal width exceeds this value implies some polydispersity in the sample provided the sample does not have specific chemical interactions with the column. As shown in our previous work, reproduced in Fig. 7,[52] our best metal cluster samples have $\Delta t_{1/2} = 0.30$–0.35 min, slightly narrower than the best available C60. Thus, there is some uncertainty ($\sim .05$ min) as to which value best represents the inherent column broadening The sub-populations of a polydisperse sample with elution times lying outside $t_e \pm 0.4/2$ will be separated from the clusters representing the signal at the apex of the peak and contain additional spectral information. Optical spectra obtained from the size-selected population eluting at the peak apex represents a single size to within the ± 2 Å resolution for the column shown. By increasing the total pore volume of the column through the addition of an identical column in series, this resolution of ± 2 Å can be increased.

In a recent paper a synthesis based upon the seminal work of G. Schmid[11] illustrates the selection and optical characterization abilities of HRSEC for strongly polydisperse samples.[44] In that paper an observation of a discrete, "molecule-like" density of states in Au cluster absorbance spectra were obtained by an on-line PDA. Specifically, the elution time of this sub-population of size-selected Au "molecules" corresponded closely in hydrodynamic size to Au($N = 13$), the smallest closed shell atomic configuration. Au clusters with approximately this size had been previously shown by us[75] and subsequently by others[49,76,77] to have both visible and NIR photoluminesence, (PL). The observed visible PL ($\sim 10^{-4}$

This journal is © The Royal Society of Chemistry 2006

Chem. Soc. Rev., 2006, **35**, 1162–1194 | 1173

quantum yield) can come from both s to d interband transitions (visible PL), or intra-d-band transitions (NIR & IR PL). The discovery of such unexpected optoelectronic properties illustrate the reason very small nanoclusters are so interesting.

In summary, SEC allows rapid, quantitative feedback concerning final cluster size, shape, optical properties and their relationship to the myriad synthetic variables affecting the average cluster size and size distribution. In addition, separate sub-populations with different size or shape can be separated in mg quantities, collected and analyzed for composition by more traditional analytical techniques such as XRF.

Absorbance spectroscopy

The absorbance spectra of passivated metal nanoclusters can be obtained *in situ* during SEC using an on-line photodiode array (PDA) with an adjustable bandwidth and wavelength range. Typical bandwidths for our system were either 2.4 nm or 4.8 nm when using a wavelength scan range of 290–795 nm. Complete absorbance spectra can be collected every 2 seconds during the chromatography.

Since a typical cluster elution linewidth is about 0.3–0.4 min, between 10–15 complete spectra are available as a function of elution time (*i.e.* size). So, in addition to the information concerning how the absorbance spectra changes with cluster size at the peak of the elution, we also can determine the spectral homogeneity or purity of an elution peak. A spectrally pure or homogeneous elution peak corresponds to one in which there is no variation in the absorbance spectral shape within the peak. Size or shape polydispersity would lead to size dependent optical absorption spectra within the elution peak.

Other characterization techniques

The need for rapid analysis techniques for inorganic nanomaterials has led us to try to adapt some modern analytical methods to study the relationship between size and optical property relationships. One very useful technique is elemental analysis of size or shape fractionated cluster solutions using X-ray fluorescence, XRF. This is a quick and easy method to verify concentrations and ratios of constituents and the separation capabilities of SEC gives more detailed information than ensemble average measurements of composition for the entire as-synthesized cluster population. The technique can be applied in solution and so is non-destructive to the clusters allowing subsequent analysis by other techniques.

TEM (described above) or X-ray diffraction, XRD, has traditionally been used to infer the nanocluster particle size. In XRD characterization of cluster size, the first maximum in the low-angle diffraction pattern can be used to obtain the average interparticle spacing. This size calculation assumes either hexagonal or cubic packing. In an actual sample, the interparticle gap depends on the organic ligand and its degree of interdigitization. One can also obtain the nanocrystallline domain size from the linewidth of individual diffraction peaks using the Debye–Scheer relation. However, defects within a cluster which make it multi-domain invalidate this type of size analysis. This makes using XRD not ideal. However, it can be applied to very small, monodomain clusters with $D_c < 2$ nm,

and has used with good precision for very monodisperse clusters.[77]

Small angle neutron (SANS), X-ray (SAXS) and dynamic light scattering (DLS), are methods that can be useful for size and size dispersion analysis for certain sizes and types of metal clusters.[78] However, since DLS uses visible light, the very strong optical absorbance by metal nanoclusters combined with weak scattering due to their small size requires very low nanocluster concentrations. These factors result in a very low signal/noise, S/N, ratio for clusters with $D_c < 4$ nm.

Since DLS measures the de-phasing of the coherent laser light due to cluster diffusion, the diffusion constant for even the smallest molecules or clusters can theoretically be obtained provided a sufficient sample collection time is allowed. For clusters as small as 2 nm this collection time for a reasonable laser power of a few tens of mW can be more than 48 h. So, the practical application of this sizing approach is limited to clusters larger than 4 nm. The hydrodynamic size of the cluster is obtained from the diffusion constant and the known solution viscosity and temperature. The shape of the intensity autocorrelation function obtained by DLS and its deviation from a purely exponential decay also provide rough estimates of the size polydispersity. However, for clusters smaller than ∼2 nm, this decay may be rapid enough to demand very fast autocorrelators and very long sampling times. Because of these practical considerations, only samples with narrow size distributions and thus nearly exponential decay of the autocorrelation function can by analyzed quantitatively.

A similar situation of low S/N exists with SANS, due to the small scattering length density difference between solvent and typical metal nanoclusters. Of the three scattering techniques, SAXS is the best approach with better S/N from metallic nanoclusters. However, to be practical this sizing approach requires an intense, energy tunable (synchrotron) X-ray source, to avoid overly long (*e.g.* 24 h) data collection times.[78] A nice example of the use of SAXS to estimate ensemble average size and size dispersion was given in the work by Shevchenko *et al.*[39] In this work the narrow cluster size dispersion and moderate size for clusters 4 and 10 nm gave SAXS data with several oscillations in the structure factor. Analysis of the sharpest of the minima and maxima in the structure factor and modeling with simple assumptions such as spherical geometry allows one to extract the average size and size dispersion. Our observations and experience with the techniques described above suggest that the most versatile approach for obtaining simultaneous optical and cluster dispersion information is SEC. We justify this assertion with the following examples of SEC of metal nanoclusters.

SEC studies of synthetic variables

Au nanoclusters

As mentioned in the characterization section above, SEC can be used to study variations of synthetic variables and their effect on the final metal nanocluster product. The high speed, precision, and high information content of SEC size/optical property analysis are crucial to synthesis protocol. This allows for a systematic study of synthesis processes in general, leading to a scientific foundation and sound predictions once the
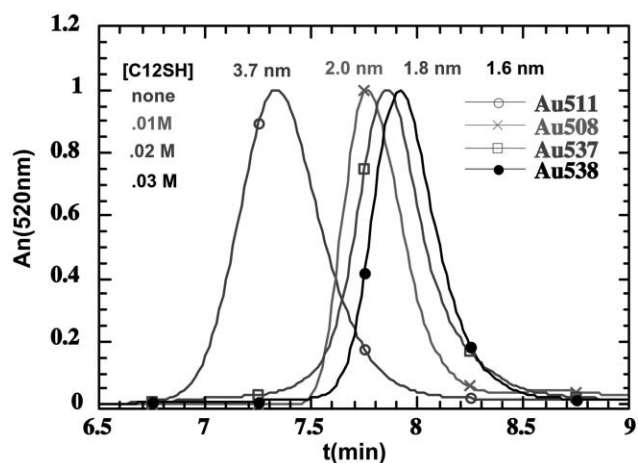
Fig. 8 Effect of dodecanethiol, C12SH concentration on the final nanocluster size and size distribution of Au nanoclusters made by NaBH$_4$ reduction of a two component TOAB–toluene inverse micelle system with [Au] = 0.01 M. The column is a polymer labs 1000 Å pore type and the mobile phase is toluene with C12SH added at 0.01 M. The SEC core sizes assume a core-size-independent 2.4 nm total organic shell and are indicated above each curve. (Reprinted with permission from Ref 44: J. P. Wilcoxon and P. Provencio, Etching and aging effects in nanosize Au clusters investigated using high-resolution size-exclusion chromatography, *J. Phys. Chem. B*, 2003, **107**(47), 12949–12957. Copyright (2003) American Chemical Society.)
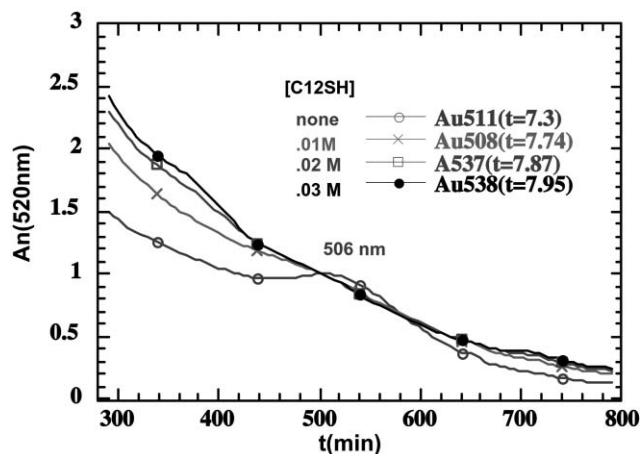
Fig. 9 Absorbance at the elution peak of each of the chromatograms of Fig. 8 illustrating the blue shift and absorbance broadening with decreasing cluster size. All the clusters are in toluene which is the mobile phase too. (Reprinted with permission from Ref 44: J. P. Wilcoxon and P. Provencio, Etching and aging effects in nanosize Au clusters investigated using high-resolution size-exclusion chromatography, *J. Phys. Chem. B*, 2003, **107**(47), 12949–12957. Copyright (2003) American Chemical Society.)

important parameters are identified. In order to do this, the influence of certain variables on the final cluster size and size dispersion must be identified.

As a first experimental example the solvent, metal precursor concentration, reductant, and inverse micelle surfactant types were fixed while the effect of alkyl thiol concentration on the final cluster size was analyzed. Fig. 8 shows the SEC chromatograms from Au nanoclusters synthesized with various amounts of dodecanethiol, C12SH, added ranging from 0.0 to 0.03 M.[44] The numbers attached to the end of ''Au'' are a sample labeling system, not an enumeration of the number of atoms in the cluster. The characteristics of each sample are shown in the figure. The highest concentration of C12SH corresponds to the smallest clusters formed. These results indicate that having more of the tightly binding alkyl thiol restricts the growth more strongly.

The complete absorbance spectra can be obtained from an on-line photodiode array (PDA) yielding absorption information throughout the elution peak. The spectra obtained at the peak apex reflect the absorbance of the majority of the nanoclusters. Fig. 9[44] shows the absorption spectra corresponding to the elution peaks of Fig. 8. They are normalized at a common value, 500 nm for each sample. A blue shift of the absorbance with decreasing Au cluster size (increasing elution time) is apparent. Non-classical features in the absorbance spectra appear as the size decreases from ~2.0 nm to 1.6 nm. This is due to the discrete density of conduction and valence band states of these gold clusters which contain only about 55 atoms. The cluster size, obtained from the elution time, of D_c = 1.6 nm corresponds very closely to this magic size. This corresponds to two fully closed shells icosohedra with N = 55 atoms first synthesized and identified by Schmid.[11] Link,

Whetten and Schaaff *et al.* have also identified this magic size using MALDI TOF mass spectroscopy.[49,76]

A second SEC analysis example involves studies of the role that the inverse micelle and solvent type play in determining the final cluster size. It has been previously shown[44] that even in the presence of a strongly binding thiol, the micellar binding to the encapsulated precursor salt has a significant effect on the final cluster size and size distribution. Fig. 10 shows the cluster size distribution obtained for nonionic, three types of cationic surfactant, and an anionic surfactant. In each case the solvent and reductant were held constant. As can be seen from this figure, there is a significant dependence of final cluster size
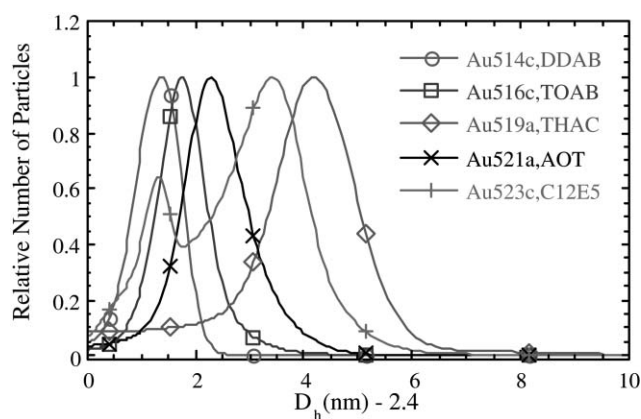

Fig. 10 Plot of the Au core size $D_c = D_h - 2.4$ obtained by assuming the previously measured total shell thickness of 2.4 nm, *vs* normalized detector response at 520 nm (relative number of particles). The surfactants used in the synthesis are indicated. (Reprinted with permission from Ref 44: J. P. Wilcoxon and P. Provencio, Etching and aging effects in nanosize Au clusters investigated using high-resolution size-exclusion chromatography, *J. Phys. Chem. B*, 2003, **107**(47), 12949–12957. Copyright (2003) American Chemical Society.)

This journal is © The Royal Society of Chemistry 2006

Chem. Soc. Rev., 2006, **35**, 1162–1194 | 1175

upon the inverse micelle surfactant type. Of course, there are other factors at play here such as competitive binding between the surfactant and/or added stabilizer with the growing cluster surface. The type of stabilizer and its complexation with the metal salt also has an effect on the final cluster size, just as is found in organo-metallic decomposition methods.

A final factor to consider is the role of precursor salt concentration on the final size and size distribution. This did not seem to be as significant a factor in the inverse micelle synthesis as in other synthesis techniques such as chemical thermolysis reactions of organometallics in coordinating organic solvents. In this decomposition approach, an increase in metal–organic precursor concentration mainly leads to greater final sizes accompanied by increased size dispersion. However, complexation to the metal may increase the nucleation rate, possibly lowering the final cluster size.

In summary, SEC studies reveal there are at least four factors that control the final nanocluster size during inverse micelle synthesis. They include: the micelle size, the binding strength of the surfactant, the amount of precursor salt used and the strength of the reducing agent used. Our examples demonstrate that SEC can be used to study each of these factors giving some insight and possible predictive ability as to size and optical properties of the final nanocluster sample.

Ag nanoclusters

Till now, we have been considering examples of the synthesis of Au nanoclusters and their size-dependent optical properties. Ag nanoclusters exhibit very distinct differences in size-dependent optical properties compared to Au. This difference is likely due to the different energies of the interband (filled d shell to conduction sp band) transition onsets in the two metals. The close proximity of the interband transition to the plasmon energy in Au, (it lies to the red of the plasmon energy), is the reason the energy damping, manifest as peak broadening, is so much greater for Au clusters than for Ag where the interband transition energy onset lies significantly to the blue of the conduction band plasmon. This makes a determination of the size-dependence of the linewidth for small Au clusters difficult (e.g. the peak simply disappears for sufficiently small size). It also gives rise to a pronounced asymmetry in the peak shape.

Significant controversy has surrounded the issue of the plasmon absorbance energy shift dependence on cluster size in the quantum size region. The details regarding the relative weight of various theoretical input parameters allows a prediction of either a blue or a red plasmon shift with decreasing cluster size. A blue shift occurs in the case of monodisperse, spherical nanoclusters of gold[79] which seems to be the general consensus based upon dozens of papers in this field.

However, the case of Ag is not as well established since both red and blue shifts have been reported. SEC and on-line optical characterization of Ag nanoclusters prepared using inverse micelle synthesis showed a clear red shift with decreasing size.[79] The magnitude of this shift was very pronounced compared to gold. Fig. 11 shows the effect of a cluster size decrease on the peak energy and linewidth of the optical absorbance of Ag nanoclusters.
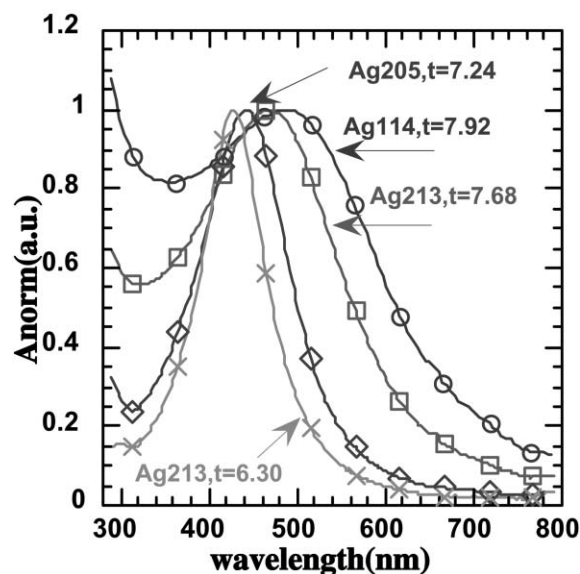

Fig. 11 Normalized absorbance, A_{norm} vs wavelength obtained during SEC separation and on-line characterization of Ag nanocluster solutions in toluene. A strong red-shift and broadening of the absorbance with decreasing size (corresponding to longer elution times) is observed. (Reprinted with permission from ref. 79: J. P. Wilcoxon et al., Optical properties of gold and silver nanoclusters investigated by liquid chromatography, J. Chem. Phys., 2001, **115**(2), 998–1008. Copyright (2001) American Institute of Physics.)

The Ag samples whose spectra were shown in Fig. 11 are all coated with an identical ligand, dodecanethiol, C12SH, which keeps the clusters from aggregating even when deposited onto a holey carbon grid and inserted into the high vacuum of an electron microscope. Fig. 12 shows a TEM of 4 nm Ag clusters illustrating the ready formation of arrays which have been termed quantum dot or nanocluster arrays (see nanocluster array section below).

The coinage metals Cu, Ag, and Au have nearly free-electrons and the condensation of these conduction band electrons into a narrow frequency range gives a resonance, or absorbance maximum to their optical spectra. The absorbance maximum occurs in the visible. If the dielectric function for a metal cluster does not depend on its size, little or no variation in the position of energy maximum of the plasmon absorbance profile is predicted to occur below a size of 10 nm. So for particles smaller than this size, as Kreibig has pointed out,[80] the absorbance band shape only changes with size if intrinsic particle effects are important. It has been established by numerous experiments that for sizes less than ~5 nm, the refractive index $n(\omega,R) \sim 1/R^2$. Thus size-dependent effects on the optical constants seem to be significant. However, this is mostly ignored in modeling of the optical absorption.

What other intrinsic particle effects are important? The assumption that the dispersion relation for the real and imaginary parts of the dielectric function (or refractive index) of a metal cluster remains that of the bulk metal is a significant error as mentioned above. The dielectric dispersion relation is usually obtained from the polarization dependence of the reflectivity of a bulk metal film as a function of frequency, ω, and so is unlikely to apply to very small nanoclusters, even if
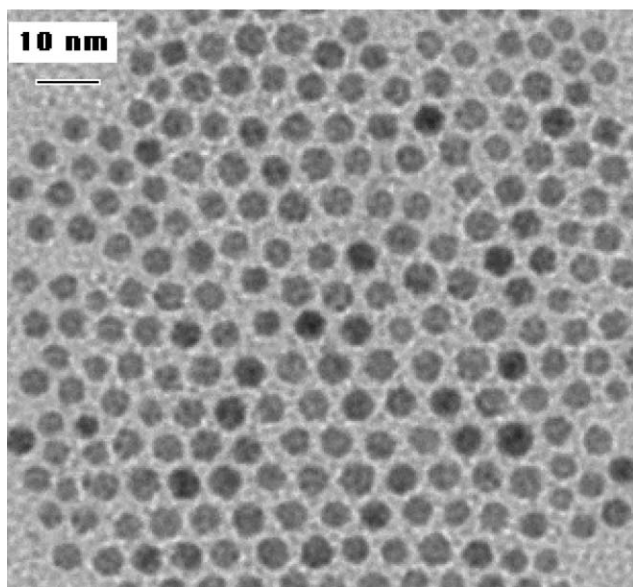
Fig. 12 TEM of Ag nanocluster with a core size of $D_c = 4.0 \pm 0.5$ nm nanoclusters stabilized with decanethiol. A solution of these clusters has an absorbance peak at 440 nm in toluene. (Reprinted with permission from ref. 79: J. P. Wilcoxon *et al.*, Optical properties of gold and silver nanoclusters investigated by liquid chromatography, *J. Chem. Phys.*, 2001, **115**(2), 998–1008. Copyright (2001) American Institute of Physics.)

there were no size dependence to n. Since a key input for the Mie calculation of optical extinction *vs* frequency is the dielectric constant as a function of frequency, a size dependence of the dielectric function invalidates any Mie calculation which assumes no size dependence of this function. In reality, the decreased electron mean path for propagation distances less than ~ 10 nm means that even in a purely classical model of absorption, the assumption that the particle refractive index is size independent cannot be correct.

Other classical effects, such as an increased electron scattering rate at the metal/dielectric interface and quantum size effects (QSE) become important for cluster sizes less than ~ 5 nm. QSE should become important when the level spacing near the Fermi level exceeds the available thermal energy. This will occur at about 400 atoms of Au, or a size of about 2.5 nm, assuming the nanoclusters to have the density of the bulk material. Since both classical effects such as the reduced free path of the electron and QSE predict a $1/R$ dependence to the resonance linewidth an observation of a $1/R$ behavior of the absorption linewidth does not, by itself, demonstrate a QSE. However, the emerging weak features in the spectra of our smallest clusters probably do indicate the onset of discrete bands which is a true QSE, since $n(\omega)$ is likely a smooth function of ω for even the smallest clusters.

A further complication in interpretation of experimental observations of size-dependent absorbance changes that invokes either classical (electron scattering) or quantum confinement (continuous bands becoming discrete) behavior occurs in the case of metals like Au and Cu. For these metals the onset frequency of the interband transitions from d-type orbitals to the sp-type conduction band is close to the plasmon

energy. So, there are major changes in the resonance energy just due to the importance of these transitions. For example, in the case of both Cu and Ag the free-electron (Drude model) Mie theory[81] predicts a resonance of ~ 9.2 eV in a vacuum ($\varepsilon_m = 1$), but the contribution of the 4d core electrons to the susceptibility shifts this to the experimental value of ~ 3.8 eV for Ag but ~ 2 eV for Cu. Perhaps, the different directions of the plasmon energy shift reported in the literature for Au and Ag with the same passivating layer, embedded in an identical media, toluene, are due to the relatively larger importance of the interband transitions in Au compared to Ag.

We summarize our findings concerning the size-dependent optical properties of Au and Ag as follows. For both Au and Ag clusters in the core size range from 8 to 1.5 nm, the absorbance peak linewidth broadens following a $1/R$ linewidth size dependence whose slope is greatest for Au. The peak asymmetry in the plasmon band shape is greatest for Au and increases with decreasing size for both Au and Ag clusters. The absorbance peak wavelength blue shifts with decreasing size for Au clusters while in the case of Ag nanoclusters a red shift is observed.

We have not discussed the huge body of literature addressing the optical properties of larger metal nanoparticles made by synthesis in aqueous or polar organic phases. There is a recent review of this work by Liz-Marzan.[1] This review features studies in which particle shape and interparticle spacing are used to alter the absorption properties of Ag, Au and alloy nanoparticles.

What are the difficulties in analyzing the optical properties of colloids made in aqueous solution as reviewed by Liz-Marzan? A quantitative analysis of the optical properties of aqueous, charge stabilized colloids, as noted by Vollmer and Kreibig, is not possible since the boundary conditions for Maxwell's equations in the presence of surface charge preclude a simple solution. So only sterically stabilized, uncharged metal clusters are appropriate for such a comparison. Additionally, as noted by Liz-Marzan in his review, it is very difficult to avoid the formation of various sizes and shapes of colloids by aqueous methods (*e.g.* sphere-like clusters will be present with prismatic, and rod-like shapes). It may be that chromatographic separation methods can help to separate out these shapes in the future, allowing more quantitative comparison between theory and experiment.

Optical properties of Ag/Au, Au/Ag core/shell and AgAu nanoalloys

There are abundant scientific reasons to investigate core/shell or alloy nanoclusters. For example, even monolayer shell coverages on the core particle atom cluster can shift the Fermi level, E_f *via* e-donation/acceptance by huge amounts (*e.g.* ~ 20–30% donation/atom blue shifts E_f by ~ 1 eV). In the case of metals with dissimilar electron affinities, interface structures may form which are similar to doping-induced depletion zones in bulk semiconductor materials. This effect may be a basis for metal rectification or spatial charge separation and thus of importance to nanocluster photocatalysis.[82–84] In view of the very interesting physics of such core/shell structures and the possibility of "reconstruction" occurring as the result of a

This journal is © The Royal Society of Chemistry 2006

Chem. Soc. Rev., 2006, **35**, 1162–1194 | 1177

heteroatomic deposition process this area of nanometals should be very fecund and deserving of investigation.

Nanoalloys of Au and Ag are nearly ideal systems to study the effects of size and composition on the optical properties of nanoparticles since they have identical covalent radii, are miscible in all proportions, and have simple fcc cubic lattice structures. However, this also means that diffraction based methods like TEM are not very useful for determining their structures. In our investigations questions which we attempted to answer include: For fixed composition and size how does the order of deposition Au/Ag *vs* Ag/Au (core/shell) affect the optical spectra? For equivalent atomic compositions and size does a random nanocluster alloy of Au and Ag differ optically from the corresponding core/shell cluster? Finally, given a fixed total size, how does composition affect the optical absorbance?

Our current information regarding these questions originates mostly from the study of charge stabilized colloids. For example, Mulvaney and co-workers prepared Ag/Au nanoclusters in water and estimated that a single monolayer of Au was enough to completely obscure the Ag plasmon absorption at $\sim$420 nm.[85] The usual assumption is that a co-reduction of the two metal pre-cursors will lead to a more random dispersion of atoms or nanoalloy while a sequential reduction using a dispersion of metal particle seeds onto which the other metal deposits heterogeneously will produce a core/shell morphology. It is often argued that even in the latter case, interdiffusion of atoms following cluster formation will produce a nanoalloy. Even with all these complexities, the optical behavior can serve as a guide to distinguish these distinct nanostructures.

Heterogeneous growth of homo and hetero-atomic metal clusters

Growth of nanocrystals in solution by any of the above three methods, (inverse micelle, chemical reduction and organometallic decomposition), relies on surfactants to control unwanted cluster aggregation during chemical reduction of ionic precursors or thermal decomposition of metal-organics. In the case of slow, controlled growth of small, ligand stabilized nanocrystals facile surface diffusion of atoms deposited on the initial cluster nuclei may create structures controlled by thermodynamic stability rather than the growth kinetics found in classical colloidal growth. As the growing clusters undergo diffusion and collisions in the solution, intercluster exchange of atoms often results in the most thermodynamically stable cluster structure. An example is the solution growth of Ir clusters as reported by Watzky and Finke.[86]

Our heterogeneous growth method involves the co-injection of an organo-metallic source of atoms with a solution containing a metal hydride reducing agent into a stirred vial containing nanocluster seed crystals.[70] As a result of the co-injection, metal atoms are deposited onto the surface of the seed nanoclusters. Several generations of clusters can be grown by using each generation as the source of seeds for the growth of the next larger generation. Lin *et al.* describe a similar growth method for Co clusters.[87] However, they used an ionic source for the Co clusters.

It is instructive to first analyze this growth process for the case of homoatomic deposition of Au on Au nanocrystals. By looking at three different growth rates, the observed sizes can be compared to those expected for complete deposition of reduced atoms onto the spherical nanocrystal seeds.[70] This type of growth can be modeled using mass conservation as verified by Teranishi *et al.* for the growth of Pd and Pt metal clusters in alcohol solutions discussed above.[62]

Heterogeneous growth of homoatomic clusters (Au atoms on Au nanocrystal seeds)

The details of Au on Au homoatomic heterogeneous growth is described elsewhere.[70] Briefly, the growth involves a metal-organic source of Au atoms containing a ligand stabilizer, such as an alkyl thiol, co-injected with a reducing agent. The injection rates are quite slow, (*e.g.* a few ml h^{-1}), to allow for the proper metal atom deposition on the seed nanocrystals. Typically, a change in color of the final product indicates that the main population of Au clusters in the solution have grown larger. Only SEC can determine that this is the only population present. Once this first generation is grown, it can serve as the seed used for generating a subsequent, larger Au/Au nanocluster sample.

The ratio of Au seed to the amount of Au deposited can also be changed to allow variation of the number of atoms deposited per growth generation. Typically, attempts to grow clusters larger than $\sim$7–8 nm using monodentate alkyl thiol stabilizers in the growth medium are more difficult and often fail due to aggregation of the clusters.

The injected Au atoms could form independent nanoclusters of a different size instead of depositing on the nanocrystal seeds as intended, or might follow a combination of both these routes. In order to analyze which routes occurs it is necessary to use a separation technique such as SEC to follow both the cluster size distribution and the average cluster size. An example of this analysis is shown in Fig. 13 exhibiting the on-line peak absorbance chromatograms of the seed and first two generations of particles grown from the D = 1.8 nm seed solution. The cluster elution is detected using the signal from the 500 nm wavelength element of the PDA in the SEC system, although the complete spectra are also collected at all times to ascertain spectral homogeneity. The core sizes, D_c, shown in Fig. 13 were obtained by subtraction of the passivating agent thickness that is present on the cluster surface.[52] These core sizes correspond to the sizes of the inorganic core as determined by TEM.

In contrast to Fig. 13, where cluster growth occurs in a 1 : 2 molar ratio of Au atoms in the form of cluster seeds to Au atoms heterogeneously deposited, Fig. 14 shows the SEC size characterization of each generation at a ratio of Au : Au = 1 : 1. This should lead to smaller increases in cluster sizes between generations as well as correspondingly smaller changes in the optical spectra. First we note that the spectra are homogeneous throughout each of the elution peaks of Fig. 14 showing the cluster population is monodisperse. This observation also demonstrates that the size, composition and shape of each generation is homogeneous. The heterogeneous growth of each generation is further confirmed by the
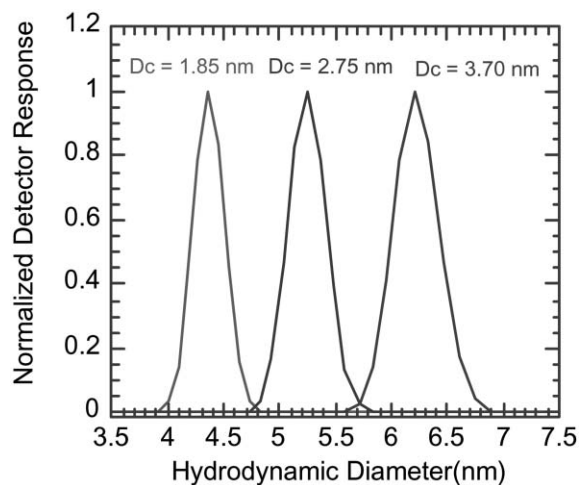
Fig. 13 Normalized absorbance detector response *vs* hydrodynamic diameter as determined by SEC *vs* for Au seed nanoclusters with a core diameter of $D_c = 1.85$ nm and two successive growth generations. The molar ratio of Au in the seed clusters to that deposited on their surface was 1 : 2. (Reprinted with permission from Ref. 70: J. P. Wilcoxon and P. Provencio, Heterogeneous growth of metal clusters from solutions of seed nanoparticles. *J. Am. Chem. Soc.*, 2004, **126**(20), 6402–6408. Copyright 2004, American Chemical Society.)

development of an absorbance maximum for the larger clusters, and its red shift with each generation as shown in Fig. 15. The data in this figure was obtained from the PDA spectrometer on-line at the elution times shown in this figure.

By plotting the nanocluster size as a function of growth generation, for predicted and actual cluster size, it is possible to test which growth route was actually taken: new cluster formation or Au metal atom deposition on the Au seed. Fig. 16 shows such a plot where the predicted growth model assumes
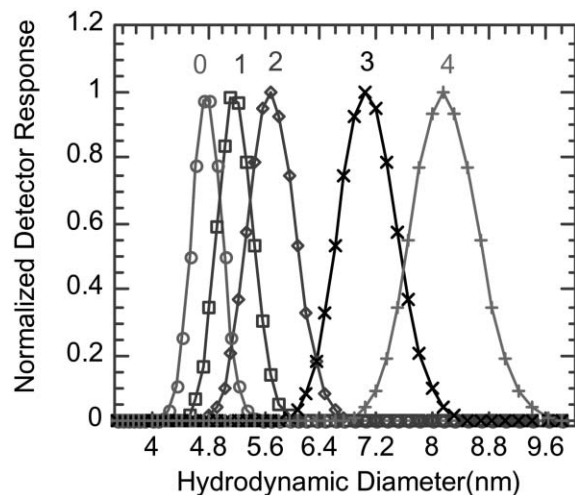
Fig. 14 Normalized PDA detector response at 500 nm *vs* hydrodynamic diameter obtained by SEC for 4 generations of clusters each serving as the seed for the growth of the next generation. The molar ratio of Au in the seed clusters to that deposited on their surface was 1 : 1. (Reprinted with permission from Ref. 70: J. P. Wilcoxon and P. Provencio, Heterogeneous growth of metal clusters from solutions of seed nanoparticles. *J. Am. Chem. Soc.*, 2004, **126**(20), 6402–6408. Copyright 2004, American Chemical Society.)
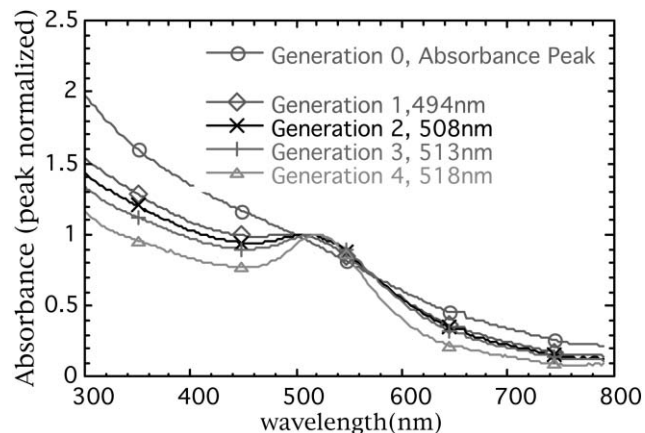
Fig. 15 Absorbance spectra taken at the peak of the elution for the cluster samples of Fig. 14. Spectra have been normalized at an identical wavelength, 500 nm, to allow comparison of their shapes. The absorbance maximum wavelength is indicated in the legend. (Reprinted with permission from Ref. 70: J. P. Wilcoxon and P. Provencio, Heterogeneous growth of metal clusters from solutions of seed nanoparticles. *J. Am. Chem. Soc.*, 2004, **126**(20), 6402–6408. Copyright 2004, American Chemical Society.)

that all the Au metal atoms (N_f) deposit out onto the seeds (N_m). As can be seen by this figure, most of the injected atoms are deposited onto the seed crystals in each case. The rate of growth is determined by ratio of atoms in the form of clusters to those in the feedstock. There are some deviations from the simple prediction for sizes larger than ~ 6 nm. This could be due to etching effects of the thiols used to stabilize the clusters during the growth process.

Using the growth approach outlined above and SEC analysis using a PDA detector we may study the effects of composition on metal cluster optical properties.
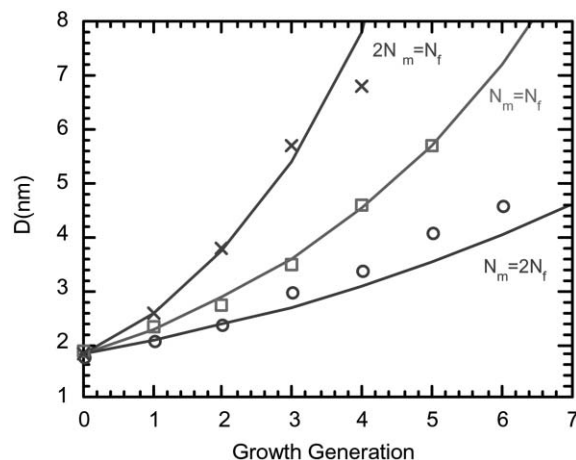

Fig. 16 Cluster size D (nm) *vs* growth generation for Au clusters. The solid curves are the predicted sizes assuming all N_f feedstock atoms deposit heterogeneously onto the N_m atoms in the form of nanocluster seeds. The symbols are the experimentally measured sizes from SEC and TEM. (Reprinted with permission from Ref. 70: J. P. Wilcoxon and P. Provencio, Heterogeneous growth of metal clusters from solutions of seed nanoparticles. *J. Am. Chem. Soc.*, 2004, **126**(20), 6402–6408. Copyright 2004, American Chemical Society.)

This journal is © The Royal Society of Chemistry 2006

Chem. Soc. Rev., 2006, **35**, 1162–1194 | 1179

Heterogeneous deposition of Ag on Au and Au on Ag (heteroatomic clusters)

By depositing a shell of a one metal onto the surface of another metal seed, the absorbance characteristics of the core metal nanoparticles can be dramatically altered. This leads to a fine tuning of the color that could be potentially useful in creating taggant materials such as metal inks. These inks would provide unique identification characteristics needed in applications such as advanced anti-counterfeiting. Reverse engineering the optical properties of such a taggant would not be possible since the order of the growth sequence will determine its absorbance spectrum. For example, a 3 nm particle of Ag on a Au core (notated, Au/Ag) with a 1 : 1 Au : Ag atomic ratio will differ in optical characteristics from a Au on Ag (notated, Ag/Au) particle with this same 1 : 1 composition. Additionally, both cluster types will differ in optical characteristics from a true alloy formed by simultaneous co-reduction of the metal salts, as described below.

As the starting point for deposition of other metals to form a core/shell type heteroatomic particle, any of the monodisperse growth generations shown in Fig. 16 can be used. As in bulk epitaxial growth, materials with the same lattice type (*e.g.* fcc) and similar atomic densities, will likely lead to the most successful outcome.

Fig. 17 shows the effect of Ag deposition on the absorbance properties of Au nanoparticles with a $D = 5.4$ nm core.[70] The red colored parent solution with an absorbance peak at 518 nm blue shifts in a systematic manner as thicker shells of Ag are formed around the core. This results in a yellow colored solution with the narrower symmetrical absorbance peak typically associated with a Ag nanocluster.

Au can also be deposited onto Ag clusters. In this case, the absorbance peak shifts in the opposite manner as shown in the
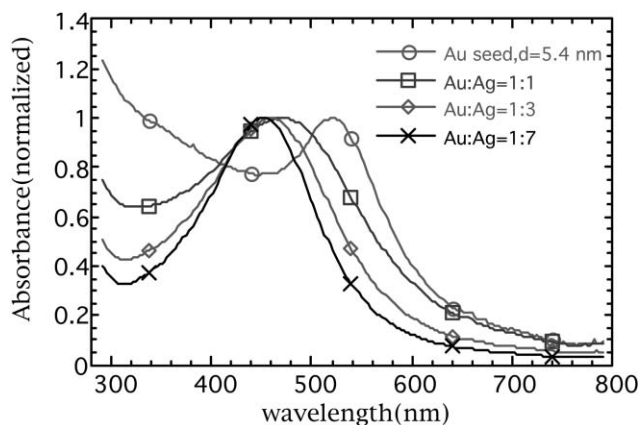

Fig. 17 Normalized absorbance *vs* wavelength obtained during chromatography for Au/Ag, core/shell nanoparticles. The effect of deposition of progressively larger amounts of Ag on Au nanoparticles with a core size of $D = 5.4$ nm is to blue shift the absorbance. The atomic ratios of Au : Ag are indicated for each case. The ratios correspond to Ag shell thicknesses (total thicknesses) of ~1.4, 3.2, and 5.3 nm respectively. (Reprinted with permission from Ref. 70: J. P. Wilcoxon and P. Provencio, Heterogeneous growth of metal clusters from solutions of seed nanoparticles. *J. Am. Chem. Soc.*, 2004, **126**(20), 6402–6408. Copyright 2004, American Chemical Society.)
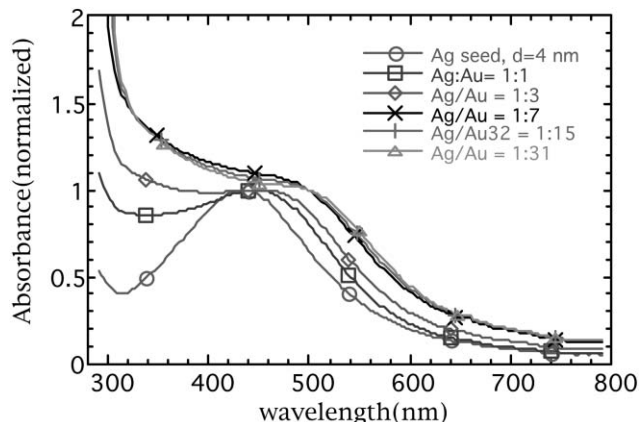

Fig. 18 Normalized absorbance *vs* wavelength obtained using during chromatography of Ag/Au, core/shell nanoparticles. The effect of deposition of progressively larger amounts of Au on Ag nanoparticles with a core size of $D = 4.0$ nm on the optical absorbance is shown. The atomic ratios of Au : Ag are indicated for each case. The ratios correspond to Au shell thicknesses (total thicknesses) of ~1, 2.5, 4, 6 and 8.2 nm respectively. (Reprinted with permission from Ref. 70: J. P. Wilcoxon and P. Provencio, Heterogeneous growth of metal clusters from solutions of seed nanoparticles. *J. Am. Chem. Soc.*, 2004, **126**(20), 6402–6408. Copyright 2004, American Chemical Society.)

example of Fig. 18. In this figure a seed population of $D = 4.0$ nm Ag was used. It is interesting to note that even when the particle has a 31 : 1 Ag : Au ratio, corresponding to a 4 nm Ag core with a total size of ~12 nm after Au deposition, the damping of the Au plasmon is much stronger than is observed in a pure Au particle of the same size.

Generally, we found that in order to ensure complete deposition of the feedstock atoms onto the seeds it was necessary to remove the inverse micelles from the seed nanocrystal solution. In contrast, Lin *et al.* showed that this was not always necessary.[87] They were able to grow successive generations of Co particles without removal of the inverse micelles. Their seeds were formed in cationic inverse micelles and they used the inverse micelle solution to grow the seeds as the feedstock for each stage of growth. TEM size measurements by Lin *et al.* showed the behavior we demonstrated in Fig. 16. However, problems did emerge when attempts were made to grow monodisperse particles much larger than 6–8 nm. This was due to both homo- and heterogeneous growth occurring which resulted in bimodal size distributions. It would be interesting to repeat these experiments using an organometallic feedstock such as cobalt acetoacetonate in toluene using purified seed nanoclusters.

Several groups have demonstrated the growth of large size clusters in the range of 12–100 nm using a seeding technique and relatively monodisperse seeds.[14,88,89] Instead of using bulky, polymer-like steric stabilizers to prevent particle agglomeration, the clusters were charge stabilized by the presence of citrate ions on their surfaces.

The synthetic protocols for synthesizing monodisperse Ag seed nanocrystals are not as well developed as they are for Au. As a result, there appears to be no studies of the optical properties of Ag core particles with a Au shell. Most of the literature focuses on alloys synthesized by the co-reduction of

metal salts in an aqueous environment[90] or core/shell particles of Ag on Au.[91,92] Also, there are difficulties calculating the optical properties of metal clusters with a charge on their surface. Thus, quantitative predictions for such colloids do not exist.[5] In the case of sterically stabilized clusters, the small sizes prevent direct comparisons to classical Mie theory.

Nanoalloys of Au and Ag and the effect of alloying on ligand binding

Bimetallic AuAg nanoclusters were first synthesized and their structural and optical properties studied using TEM, UV/Visible spectroscopy and X-ray photoelectron spectroscopy, XPS by Han *et al.*[93] In this work, co-reduction of KAuCl$_4$ and KAg(CN)$_2$ in the presence of a cationic surfactant, which forms inverse micelles in toluene was used to synthesize nanoalloys. A ratio of AuCl$_4$: Ag(CN)$_2$ of 3 : 1, 1 : 1 and 1 : 3 produced particles with an average TEM size of 4.1 nm in all cases. A systematic red shift of the absorbance maximum from 419 (pure Ag) to 522 nm (pure Au) was reported. This shift varied linearly with atomic fraction of Au. However, this atomic fraction in the clusters used in this analysis exactly matched that of the precursor atomic ratio, an unlikely outcome in our opinion. Since the Au salt undergoes a more complete reduction process under the aqueous borohydride reduction conditions described, we would expect a higher Au : Ag ratio in the particles than in the precursor salts. The XPS technique used for analysis of cluster composition will simply measure the ratio of the non-volatile salts, even if incomplete reduction occurs, so the fact that this XPS ratio agrees with that of the precursor solution doesn't mean that individual clusters also have this ratio.

An interesting observation made by Han and co-workers was that the presence of the Au precursor salt seemed to facilitate the reduction of the Ag salt. They acknowledged this reduction was difficult to achieve using sodium borohydride. So, one might expect a Au core nanocluster with Ag atoms near its surface under the experimental conditions used for their synthesis. They argue that, from the absence of separate absorbance peaks corresponding to Au and Ag, the clusters formed were most likely a homogeneous distribution of Au and Ag atoms. This inference shows the critical role the optical properties play when detailed nanostructure is difficult to obtain. One must also consider the fact that interdiffusion of Au and Ag atoms in small clusters may be quite easy even at room temperature, so even if atomic segregation occurs initially, a more random distribution or indistinct interface may exist when optical measurements are obtained. It is certainly true that the spectra shown in this work differ from our results on core/shell Au/Ag nanoclusters where the presence of larger amounts of Ag leads not only to a blue shift in the peak absorption, but a narrower absorption peak width for a fixed size cluster. Instead, they find nearly identical peak shapes as a function of Ag : Au ratio.

Nanoalloy clusters can be made by dissolving precursor salts such as NaAuCl$_4$ and AgNO$_3$ in a suitable inverse micelle solution. These salts are then co-reduced using a reducing agent chosen to have approximately the same reduction kinetics for each metal precursor type. This avoids pre-nucleation of one material over the other, which would result in a core/shell nanostructure as results from sequential reduction of the salts. Selection of such a reducing agent for a general choice of metal salts can be difficult in practice.

Just as SEC can be used to study synthetic variables and ligand binding, it can also be used to determine the relative binding strengths of ligands (such as thiols of various sizes) to specific metal types (Au *vs* Ag in the alloying process). In the case of pure Au nanoclusters it was found that no thiol exchange occurs for CkSH, k = 6,10,14 even when there is an overwhelming excess of the alternate thiol present in the mobile phase.[44] However, Ag nanoclusters exchange thiols completely with the C12SH in the mobile phase, eluting at a single peak time independent of the initial thiol attached to the surface.

Nanoalloys of a 1 : 1 Au : Ag composition and common core size (2.0 nm), elute during SEC at distinct times corresponding to the organic shell thickness as shown in Fig. 19.[94] The effect of alloying Ag with Au eliminates ligand exchange. There are two possible reasons for this. First, thiol-to-metal binding strength is affected by the change in interatomic coordination and bonding distance in a spherical cluster alloy of Au and Ag (denoted, AuAg). Secondly, and equally likely, the Au sites at the surface of the metal nanoalloy allow the thiol to preferentially bind to these sites. This AuAg nanoalloy binding behavior has interesting applications in catalysis where small amounts of metal atoms in a majority phase (*e.g.* Co in MoS$_2$ hydrodesulfurization catalysts[95,96]) have been shown to impact the catalytic activity through alterations in the Mo to substrate binding strength.

There are differences in the hydrodynamic cluster size shown in Fig. 19 due to the differences in alkyl chain length differences. Still, the optical spectra of each 1 : 1 AuAg nanoalloy are indistinguishable from one another as demonstrated by the elution peak apex absorbance spectra of
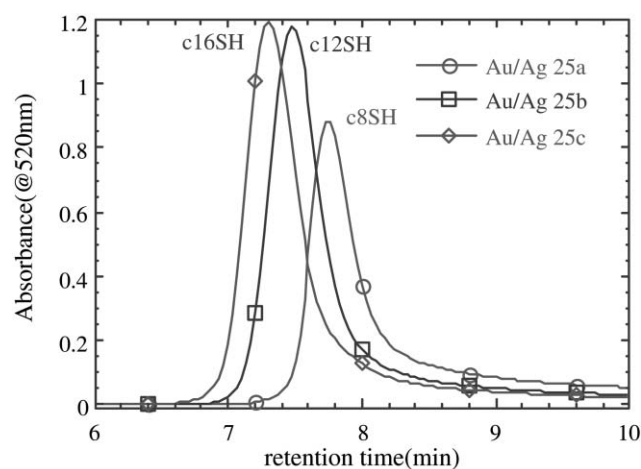

Fig. 19 Effect of organic shell on the total hydrodynamic size of AuAg alloy nanoclusters formed by co-reduction of the precursor salts in inverse micelles. (Reprinted with permission from ref. 94: From "Quantum Dots Made of Metals: Preparation and Characterization", by J. P. Wilcoxon, in *Dekker Encyclopedia of Nanoscience and Nanotechnology*, Taylor and Francis, 2004, pp. 3177–3202. Copyright (2004) Routledge/Taylor & Francis Group, LLC.)

This journal is © The Royal Society of Chemistry 2006

Chem. Soc. Rev., 2006, **35**, 1162–1194 | 1181

Fig. 20.[94] For similar sized nanoparticles of pure Ag the plasmon would occur at 460 nm, while there would be no discernible plasmon peak due to damping effects in a pure Au sample of this size. All our experiments demonstrate that the optical properties of small noble metal nanoclusters are dramatically affected by alloying. There is clear evidence of a significant change in optical properties compared to pure metal nanoclusters of equal size.

An interesting behavior to investigate using SEC is the change in the optical absorbance properties of a nanoalloy as a function of cluster size. It is difficult to predict which direction the plasmon energy will shift. We already know that the plasmon of a pure, spherical Ag nanocluster will red-shift with decreasing size, while the plasmon peak of a pure Au nanocluster will exhibit a blue shift. Fig. 21[94] shows the peak apex absorbance spectra of a 1 : 1 AuAg nanoalloy. It can be seen that the plasmon blue shifts with decreasing size. This shows that the Au component of the nanoalloy dominates its optical behavior. Even though an increased damping exemplified by the broadening of the peak of the plasmon occurs with decreasing size, a distinct absorbance maximum is still observed for 1.8 nm clusters. This may be due to the silver component, leading to a decrease in the dissipation of the electron plasmon oscillations.

It is important to highlight the very big difference between the optical absorbance behavior of the 1.8 nm AuAg nanoalloys and the pure nanometals of the same size, coated with the identical organic thiol. Fig. 22 [94] shows the optical spectra from pure nanometals to be compared to the optical spectra of the nanoalloys from Fig. 21.

The reader should understand that developing a complete theoretical explanation of the nanoalloy optical behavior in the quantum size regime should be quite difficult especially considering the extent of damping and energy shift which cannot be predicted currently even for pure metal nanoclusters.
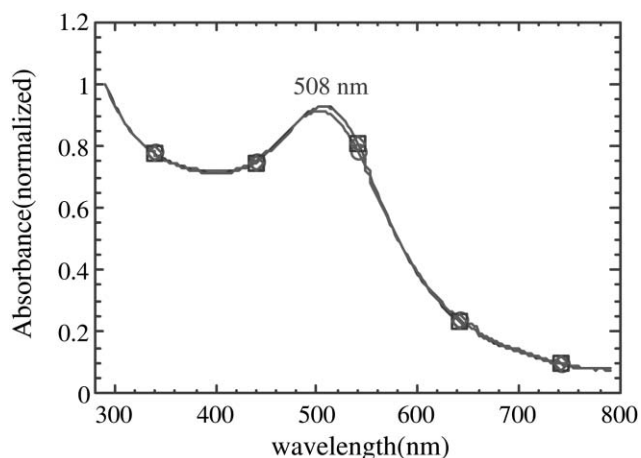

Fig. 21 The peak apex absorbance spectra of a D_c = 2.4 and 1.8 nm 1 : 1 Au/Ag alloy. (Reprinted with permission from ref. 94: From "Quantum Dots Made of Metals: Preparation and Characterization", by J. P. Wilcoxon, in *Dekker Encyclopedia of Nanoscience and Nanotechnology*, Taylor and Francis, 2004, pp. 3177–3202. Copyright (2004) Routledge/Taylor & Francis Group, LLC.)
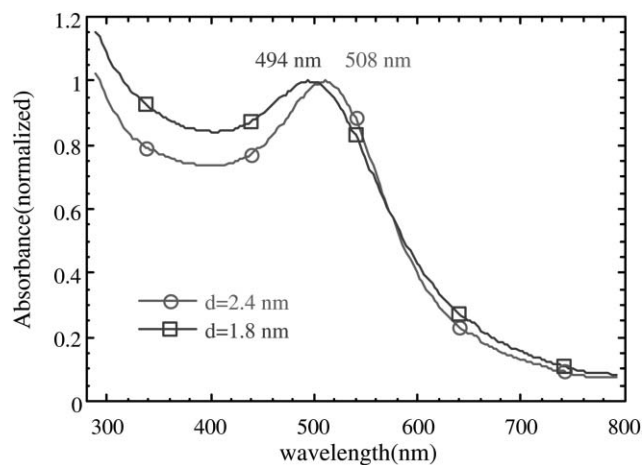
Base metal nanoclusters—Co, Fe, and Ni

Using thermal decomposition as a route to the formation of base metal colloids has been reviewed by Murray *et al.*[9] This method uses metal carbonyl decomposition in the presence of a surfactant or polymer and is done in a relatively high boiling point solvent such as xylene, diphenyl ether, or triethyl benzene. This approach usually produces relatively large nanoclusters with sizes greater than 4–5 nm. Unfortunately, the resulting clusters have significant nanocrystalline defects and exhibit polydispersity requiring post-reaction size selection. Improvements in the synthesis methods have successfully addressed the issue of polydispersity but since decomposition occurs very rapidly there are still significant defects which

Fig. 20 The peak apex absorbance spectra of a D_c = 2.4 nm 1 : 1 AuAg nanoalloy. (Reprinted with permission from ref. 94: From "Quantum Dots Made of Metals: Preparation and Characterization", by J. P. Wilcoxon, in *Dekker Encyclopedia of Nanoscience and Nanotechnology*, Taylor and Francis, 2004, pp. 3177–3202. Copyright (2004) Routledge/Taylor & Francis Group, LLC.)
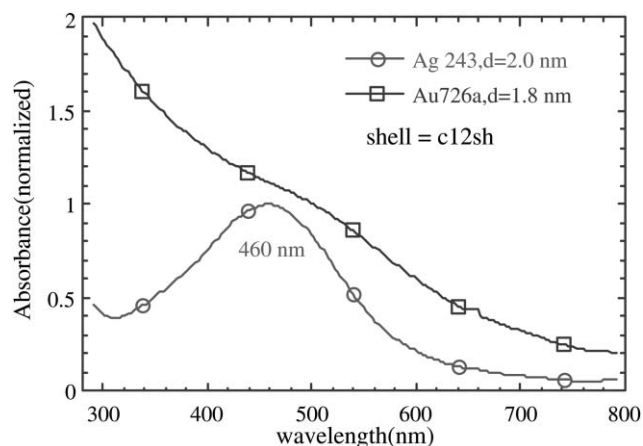

Fig. 22 The normalized peak apex absorbance spectra of Ag and Au metal nanoclusters. Both clusters are ligated with dodecanethiol, C12SH. Compare to the spectra of Fig. 21. (Reprinted with permission from ref. 94: From "Quantum Dots Made of Metals: Preparation and Characterization", by J. P. Wilcoxon, in *Dekker Encyclopedia of Nanoscience and Nanotechnology*, Taylor and Francis, 2004, pp. 3177–3202. Copyright (2004) Routledge/Taylor & Francis Group, LLC.)

result in poor magnetic response compared to the bulk counterparts (for example, ~ 0.2 of M_{sat} for 6 nm hcp Co). Thermal annealing of the clusters to remove the defects often leads to aggregation or sintering of the clusters.

The work of Chaudret and co-workers,[36,37] reviewed earlier in this paper, employing hydrogen reduction under mild conditions of temperature and pressure can produce small, 1–2 nm clusters but not larger ones. Co magnetic clusters synthesized by this method have magnetic responses slightly exceeding those of the bulk materials and thus are closest in properties to bare clusters produced in the gas phase without any organic ligands. One might conclude from this observation that the organic ligands at the cluster surface are responsible for the poor magnetic response observed and reviewed by Murray. However, our experiments, outlined below, indicate this cannot be the sole reason for the weak magnetic response from clusters synthesized *via* organometallic decomposition.

Depending on the synthetic approach chosen, it has been discovered that different structural phases of base metal nanoclusters can be produced. One of the first examples of this phenomenon was given in a paper describing the effects surfactants have on the formation of either α-Fe (bcc phase) or γ-Fe (the high T, fcc phase) using the inverse micelle process.[43] It was later shown by Sun *et al.*[97] that when Co is reduced by Superhydride (lithium triethylborohydride) at high T, an ε-Co phase was formed. This phase is a complex 20 atom per unit cell structure related to β-Mn. Sun *et al.* also showed that by annealing these Co nanoparticles at temperatures greater than 300 °C, they could be converted to the hcp phase. The ε-Co phase change was useful but even the hcp phase nanoclusters exhibited a significantly lower magnetic response than bulk hcp Co.

Petit and Pileni *et al* have explored the magnetic behavior of nanosized Co synthesized using the inverse microemulsion approach using an anionic surfactant, AOT.[98] It was claimed based upon XRD that the nanostructure of 5.8 nm (TEM size) particles was fcc. However, the XRD was too broad to justify this conclusion. Sharp X-ray reflections corresponding to fcc structure only emerged upon heating the sample to 500 °C. Under these conditions extensive sintering of the particles would occur, as demonstrated by the sharp lines in their XRD data. A phase change in nanostructure is also quite likely as reported by Sun and Murray upon heating FePt clusters to a similar temperature.[10] So, it is likely the particles had a disordered hcp structure as synthesized. Because the synthesis by Petit *et al.*[98] was performed in the presence of water using NaBH$_4$, it is very probable that Co$_2$B also forms. In the water-free inverse micelle synthesis described below this chemistry is not possible and only zero-valent Co clusters may form. As in the case of Co clusters synthesized *via* metal organic routes, the magnetic response was only 50% of that of bulk HCP Co. Though not discussed in detail, a reduction due to Co$_2$B formation and/or defects in the nanostructure might explain the poor magnetic response and lack of a sharp blocking transition in these clusters. Petit *et al.* have also made some of the only measurements of Co clusters in the form of thin films. Their results in this area will be reviewed subsequently.

It has been difficult to rationalize why a low saturation magnetism (M_{sat}) of 8 emu g^{-1} ($\sim 5\%$ of the bulk value for Co)

was observed by Murray as the cluster size was decreased to 3 nm even for nanocrystalline hcp Co synthesized *via* thermal decomposition.[9] The M_{sat} for even for the largest $D_c \sim 11$ nm Co clusters was only about 60% of the bulk. An M_{sat} value of $\sim 60\%$ of the bulk is also the maximum measured for nanocrystalline α-Fe. A reasonable question is whether this lowered magnetic response is due to the surface, nanocrystalline defects, spin canting effects, or inadvertent formation of an oxide layer? It is true that a lower density oxide is evident in TEMs of these nanoclusters but its thickness may not be sufficient to explain the reduced magnetic response. A more a likely explanation is poor spin exchange coupling due to nanocrystalline defects and/or spin canting near the surface.

Surprisingly, 1–2 nm Co nanoclusters with more surface area synthesized by the slower growth typical of the water-free inverse micelle approach have a saturated magnetic response greater than bulk values by 10–15%.[99] This implies all the spins contribute to the magnetism, including those at the cluster surface. This unexpected result likely depends on the chemical nature of the surfactant used to stabilize the nanoclusters combined with the long time permitted for room T, fully dispersed phase, structural "reconstruction" of the atoms on the cluster surface.

Cluster surface reconstruction *via* atomic exchange can result in changes in the magnetic response with sample age. For example, Fig. 23 shows magnetic response data from freshly synthesized 1.8 nm, Co nanoclusters. Data represented by the open circles in Fig. 23 have low magnetic response, only about $\sim 20\%$ of the bulk. Upon sample aging under ambient conditions, under Ar atmosphere in a dilute solution of decane, an increase in magnetic saturation from ~ 44 emu g^{-1} or 0.47 μ_B atom^{-1} after one day to 187 emu g^{-1} or 1.98 μ_B atom^{-1} after 30 days (values for bulk hcp Co are 161 emu g^{-1} or 1.71 μ_B atom^{-1}) is observed. The improvement in the magnetic response with sample age in small Co clusters is also observed in Fe and Ni clusters synthesized using the same
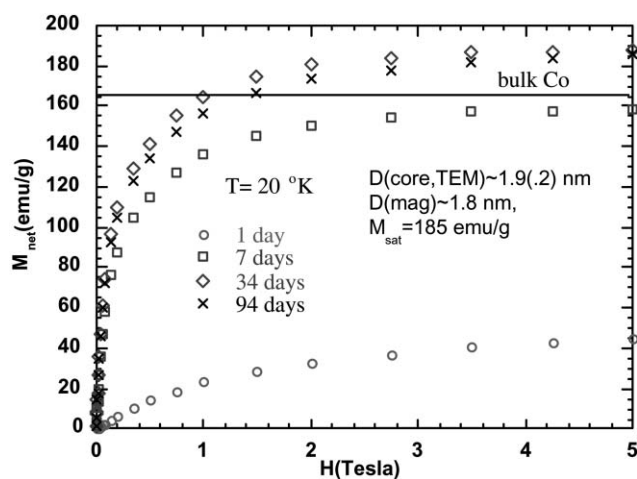

Fig. 23 Net magnetic response, M_{net} of Co, $D = 1.8$ nm clusters in decane *vs* external applied field, H as a function of sample age. The solid line shows the saturation magnetization of bulk Co. (Reprinted with permission from ref. 99: J. P. Wilcoxon, E. L. Venturini, and P. Provencio, *Physical Review B*, 2004, **69**, 172402. Copyright (2004) American Physical Society.)
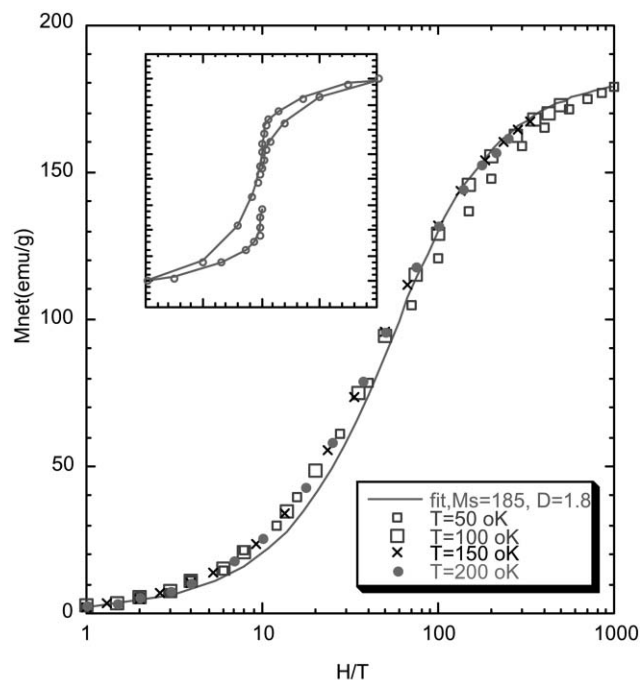
Fig. 24 Magnetic response data from a $D = 1.8$ nm dilute, frozen solution of Co clusters for temperatures well above the blocking T closely follow the Langevin prediction, (solid curve). The inset shows the low field data obtained at $T = 5\ °K$, slightly below the blocking $T_B = 7.5\ °K$. (Reprinted with permission from ref. 99: J. P. Wilcoxon, E. L. Venturini, and P. Provencio, *Physical Review B*, 2004, **69**, 172402. Copyright (2004) American Physical Society.)

non-ionic surfactant system. The key seems to be the relatively weak interaction of this multi-dentate ligand with the cluster surface which allows the atoms (spins) to fully participate in the magnetic response to the external field.

These Co clusters behave like ideal magnetic dipoles as demonstrated in Fig. 24. The spin blocking temperature, T_B for such Langevin dipoles is a product of the magneto-crystalline anisotropy and the magnetic volume or total number of atoms. Thus, the observation that the dramatic increase in magnetic moment atom^{-1} is not accompanied by a significant change in the blocking temperature, T_B, implies that this large increase in magnetic response is due to diffusion and restructuring of surface Co atoms, rather than changes in either internal structure or magnetic volume (number of atoms per cluster). This cluster restructuring process is analogous to that found in transition metal clusters where exchange of surface atoms leads to a narrowing of the cluster size distribution with age. In the case of these Co clusters the surface restructuring results in a more stable and strongly magnetic cluster. After a month of aging, no further changes in magnetic response occur as shown in Fig. 23.

Our solution results are consistent with previous experiments by Billas *et al.* on very small Co, Fe, and Ni nanoclusters made using their cluster beam approach in a vacuum and studied by magnetic deflection combined with mass selection.[30] These experiments showed that, as a result of fewer nearest atomic neighbors in smaller clusters, the magnetic moment per atom increased. The basic idea is that less hybridization occurs with fewer neighbors and thus less transfer of spin density into the upper, magnetically split d states. Transfer of spin density by any process into these states should lower the magnetic moment per atom. The fact that magnetic clusters can be grown in solution with high magnetic response and no hysteresis enables potential applications requiring no energy dissipation such as transformers, magnetic read heads, and high RF inductors.

Our 1.8 nm Co nanoclusters obey Langevin spin dynamics as expected for dilute, independent superparamagnets. The solid line in Fig. 24 is the best fit to the Langevin equation describing independent, magnetically isolated dipoles with a spherical magnetic size of $D = 1.8 \pm 0.1$ nm, a value in close agreement with the TEM cross-section of 1.8 ± 0.2 nm. There is a small systematic deviation from simple behavior closer to the blocking temperature. This is similar to that observed for more concentrated 1.6 nm Co nanoclusters in polymers as described by Osuna and Respaud *et al.*[36,100] The inset of Fig. 24 shows that below the spin blocking temperature, hysteresis is observed and a remnant magnetic moment at zero applied field is also found. The temperature required to observe this behavior is incredibly small due to the small size of these clusters.

The improvement in magnetic response with aging shown in Fig. 23 may be due to the large number of non-equilibrium surface positions for as-synthesized Co clusters of such small dimensions and surface restructuring due to exchange of atoms between clusters when they collide. This is only possible in solution and does not occur in a frozen, solid matrix. If our restructuring conjecture is true then any chemical/electronic change to these surface atoms should have a strong influence on the magnetic response.

Fig. 25 shows how sensitive the surface of these 1.8 nm Co clusters are to different surface constituents and the effect
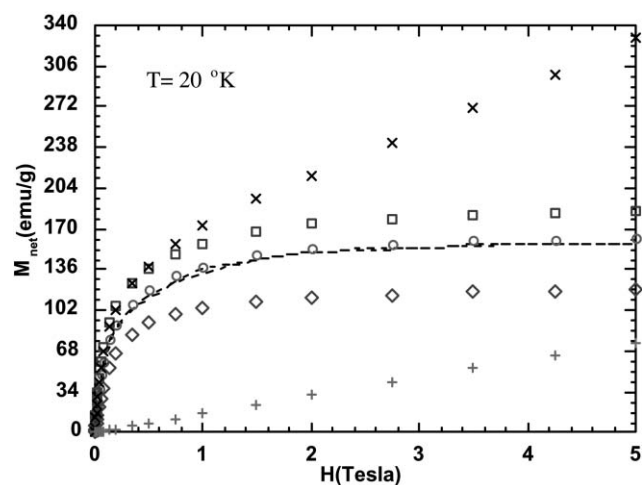

Fig. 25 Magnetic response of frozen solutions of 1.8 nm Co nanoclusters in decane when exposed to identical concentrations of surfactants. Crosses are hexadecylamine, squares, oleic acid, circles, tri-octyl phosphine, diamonds, dedecanethiol, and crosses, oxygen exposure for several days. The dashed curve is the parent sample stabilized with a non-ionic surfactant. (Reprinted with permission from ref. 99: J. P. Wilcoxon, E. L. Venturini, and P. Provencio, *Physical Review B*, 2004, **69**, 172402. Copyright (2004) American Physical Society.)

ligand-induced changes in surface chemistry have on the saturation magnetism. Equivalent amounts (0.01 M) of chemically different surfactants were added to the Co solution after 7 days of annealing in the glovebox at room T. These surfactants are described in the caption to this figure. The saturation magnetic response, M_s was equal to that found in bulk hcp Co prior to addition of these surfactants. Displacement of the original nonionic surfactant by the new surfactants was observed to alter the magnetic response in most cases.

The surfactants used in this study are the same ones typically used to sterically stabilize larger Co clusters grown by high T thermal decomposition of organometallic precursors.[9] Our results suggest that the effects on the magnetic response of strongly magnetic clusters are too small (10–20% reduction, at most), to explain the results of Murray et al[9] or Petit et al[98] described previously. However, oxidation of Co clusters by air exposure changes both the shape of the magnetic response curve and its high field response as shown in Fig. 25. Also relevant to claims of metal cluster stabilization by phosphine are our observations on the effect of addition of tri-octyl phosphine, TOP, to strongly magnetic Co clusters. We found TOP had no effect on the magnetic response, indicating that it may not bind strongly at any of the surface sites on the Co clusters. We believe this negative binding indication is consistent with the unoxidized nature of our cluster surface. As noted previously, clusters formed by high T decomposition using organo-metallic precursors typically have oxidized surfaces which are stabilized with oleic acid, oleyl amine or TOP. The other surfactants shown in Fig. 25 have little effect on the low field magnetic response but induce major changes at high field.

Dodecanethiol and hexadecylamine exhibit the largest changes in large field magnetic response. Both of these surfactants are known to bind strongly by donating electron density into empty metal orbitals in a variety of metals yet have opposite effects on the magnetic response in this case. Dodecanethiol lowers the magnetic response from $\sim$170 emu g^{-1} to $\sim$110 emu g^{-1} at H = 5 Tesla whereas hexadecylamine addition results in a strongly enhanced moment with a nearly linear high-field response and a value of over 300 emu g^{-1} at our highest field, H = 5 T. In the case of dodecanethiol, this observation might be explained by assuming that electron donation by the lone pair of electrons on the sulfur into the empty d orbitals of the Co atoms at the surface lowers the net spin of these atoms. Even though the amine has very different behavior at high field compared to the thiol, at low fields, the shape of the magnetization curve closely follows that of the other samples with the other surfactants. There is currently no reasonable explanation for the magnetic behavior observed upon addition of the primary amine.

Osuna et al. have shown that binding of molecules like CO to the surface of 1.6 nm Co nanoclusters in a polymer can significantly reduce M_s to a value of 55 emu g^{-1}.[36] However, the behavior shown by hexadecylamine in Fig. 25 has not been observed before and it is quite difficult to understand. Oxidation of these Co clusters to paramagnetic Co(II) ions yields a very different magnetic response shape with M_s of only $\sim$100 emu g^{-1} at 5 T and is not a viable explanation. It was found that our Co/hexadecylamine data can be fit to a two-component sample containing Co clusters (dominant at low fields) and a paramagnetic species with a moment of a few μ_B. This behavior is similar to the heterogeneous core-shell data reported by Chen et al.[101] In that work the shell was attributed to the formation of cobalt boride at the surface due to the use of NaBH$_4$ as the reductant. This is not possible in our case where there is no water present

Petit et al[98] claim on the basis of modeling of their SAXS data from Co clusters that a core/shell model of Co/Co$_2$B does not describe their data as well as a homogeneous Co nanocluster model. However, a pure sub-population of Co$_2$B clusters, even representing the majority of the clusters is still possible in their experiments since a significant amount of water was present during the reaction as in the case of Chen and co-workers. Co$_2$B would have reduced magnetic response compared to bulk hcp Co, just as observed by them.

Effect of cluster alloying with magnetic and non-magnetic metals

Heterogeneous growth methods (i.e., deposition of atoms) developed for transition metals in solution can be applied to magnetic "core" nanoparticles of Co, Fe, and Ni. However, due to the oxygen sensitivity of these clusters the process must be carried out under inert atmosphere. It is possible to deposit either magnetic atoms (Co, Fe, Ni) onto these seeds clusters or non-magnetic atoms (Ag, Pt). We have chosen to investigate deposition of Ag and Pt. To form nanoalloys of the same composition, a co-reduction of Fe and Pt precursor salts using a very strong reductants such as LiAlH$_4$ is employed. Magnetic response measurements provide feedback regarding the nanostructure resulting from these disparate synthetic methods.

As an example of the information obtained by this approach, Fig. 26 shows the net magnetic response of a solution of pure, 3 nm Fe seed particles after deposition of Ag and Pt atoms onto the surface. This is compared to two nanoalloys of Fe with Ag and Pt of approximately the same size (i.e., blocking T) and composition. It is observed that the saturation magnetism is substantially enhanced in the alloys but quenched in the core/shell nanostructures. In the case of the FePt nanoalloy, the saturation magnetism exceeds that of bulk Fe and the clusters are superparamagnetic above 10 °K.

Interestingly, deposition of magnetic atoms such as Co on these Fe seeds results in quenching of the magnetic response. This observation illustrates the important role of the contribution of surface spins to the magnetic response for such small clusters. Apparently, the deposition process produces a disordered surface which requires annealing to restore the magnetic response. In fact, mild annealing of a solution of these clusters at just under 100 °C for three days restores most of the magnetic response. Overcoming this deposition problem in these magnetic systems should provide a systematic method for forming increasingly large magnetic clusters with good structural order and magnetic response.

Co clusters synthesized by the inverse micelle method using cationic surfactants and then aged can also show enhanced magnetic response at high fields as shown in Fig. 27. Just as
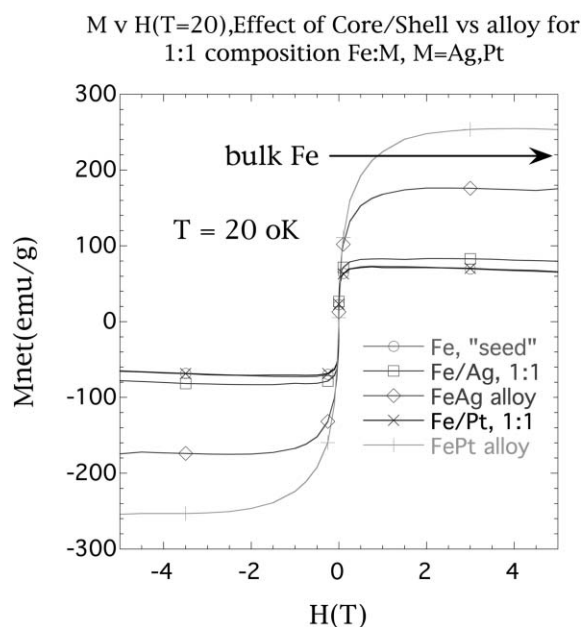
This journal is © The Royal Society of Chemistry 2006

Chem. Soc. Rev., 2006, **35**, 1162–1194 | 1185

M v H(T=20),Effect of Core/Shell vs alloy for 1:1 composition Fe:M, M=Ag,Pt

Fig. 26 The net magnetic response, M_{net} vs the external applied field, $H(T)$, in tesla, for pure Fe nanoparticles with d = 3 nm, core/shell particles and alloys. Both have a 1 : 1 atomic composition and blocking temperatures of around 9 °K. (Unpublished data.)

interesting as this enhanced magnetic behavior is the effect of deposition of additional Co magnetic atoms onto the cluster surface. This deposition quenches the magnetic response. HRTEM of such clusters still shows well ordered atomic lattice planes, so the effect must be occurring entirely at the cluster surface. However, the behavior differs from that of a simple solution of Co(II) ions as shown in this figure, so oxidation of Co(0) to Co(II) is not occurring.
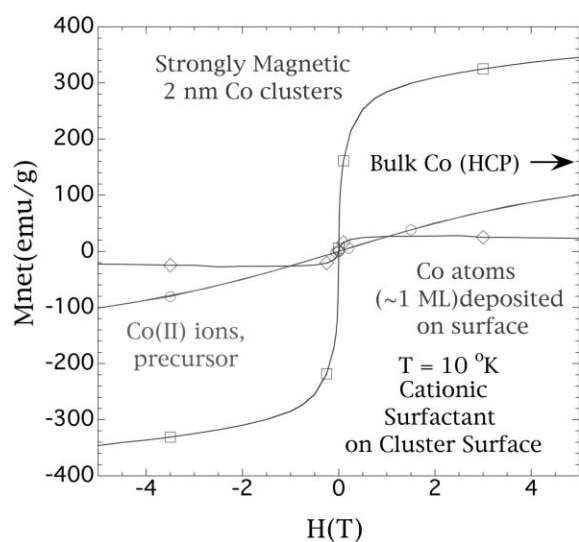
Fig. 27 Net magnetic response of 2 nm Co clusters vs applied external field H (teslas). The strongly magnetic seeds have their magnetic response quenched when ~1 monolayer of additional Co atoms is deposited in solution. The magnetic response of the precursor Co(II) ions is shown for comparison. (Unpublished data.)

Nanostructure of Sn

An interesting nanocluster material that exhibits a phase change upon decreasing the particle size from ~8–10 nm to ~2–3 nm is tin (Sn). The particle size change is achieved by using a stronger binding surfactant ligand to form smaller clusters. We wondered if this size change is accompanied by a change in nanostructure? The question was motivated by the fact that, in bulk form, tin transforms from the metallic (β-phase) to the semiconductor (α-phase) at low temperatures (~13 °C).[102,103] This transition is very difficult to achieve without the degradation of the structural properties of metallic tin, i.e., it disintegrates into a powder. However, we discovered the β (room temperature) to α (low temperature) phase transition can occur more readily upon synthesis of Sn nanoclusters using the inverse micelle approach. Fig. 28 a–c show a TEM, selected area electron diffraction, (SAD), pattern and a chart of the d spacings for α-Sn, respectively. As can be seen from Fig. 28b, the d-spacing of the 2.5 nm Sn nanocluster sample is consistent with that of the d-spacing chart for α-Sn. This is an especially interesting discovery since the synthesis of these nanoclusters was done at room temperature. The role of the surfactant in controlling the phase is very similar to that found for Fe by ourselves[43] and Co by Murray et al.[9] However, the limited role of the surfactant in controlling the nanostructure of CoPt₃ was noted earlier in our review of the analysis of the work by the Weller group.

The formation of α-Sn is very much dependent upon the type of surfactant used along with the rate of reduction. In many cases, the use of the chemically incorrect surfactant led to the immediate formation of the metallic phase, β-Sn.

The α-Sn nanoclusters exhibit interesting optical properties especially in the mid to far infrared. This could lead to possible applications utilizing infrared absorption properties. More details of this work will appear in future publications.

Formation and physical properties of metal nanocluster arrays

Most of the studies of cluster physical properties assume no interaction between clusters since they are separated by large distances (i.e. many particle diameters) in dilute solution. For optical properties this means the electromagnetic scattering from one cluster does not affect that of other clusters in solution, while for magnetic clusters it means the local field is just the external applied field and the magnetic response of a cluster is unaffected by other clusters. The total response is just the sum of individual cluster responses. If clusters are allowed to deposit onto a substrate to form a close packed film then cluster interference effects will be important in the response to an external optical or magnetic field.

Despite the difficulty in analyzing and understanding these complexities, the practical fabrication of films of ordered metal nanoparticles would allow scientists to produce substrates for surface-enhanced Raman scattering (SERS),[104] optical gratings,[105,106] anti-reflective surface coatings,[107] selective solar absorbers,[108] and data storage and microelectronics devices.[109] So, there has been considerable work to study how to make films of clusters and to analyze their degree of order.

(a)

(b)
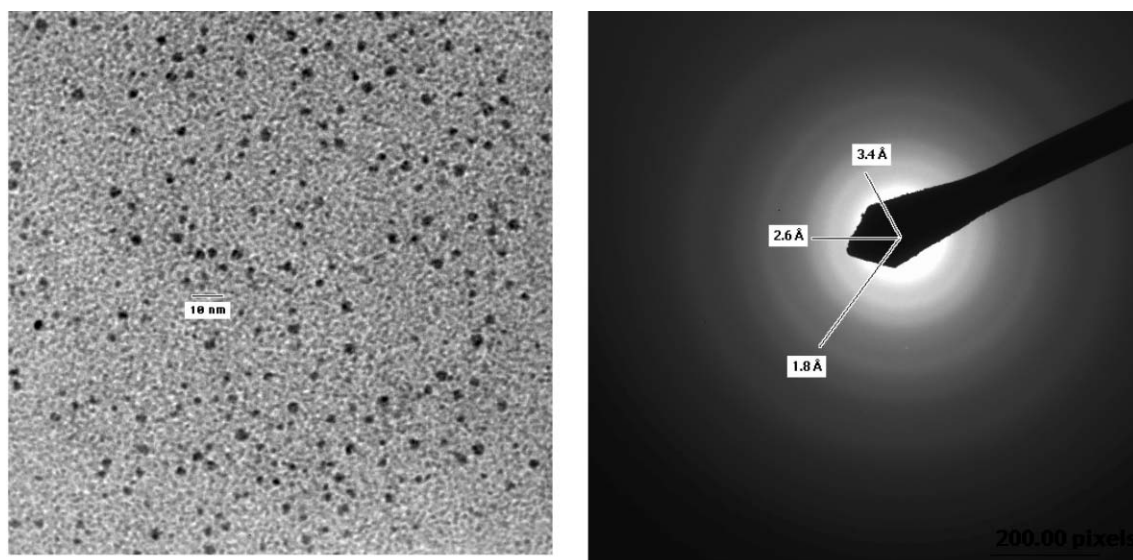
α-Sn		β-Sn	
d(Å)	**hkl**	**d(Å)**	**hkl**
3.73	111	2.915	200
2.28	220	2.793	101
1.95	311	2.062	220
1.61	400	2.017	211
1.48	331	1.659	301

(c)

Fig. 28 (a) TEM of α-Sn nanoclusters ~2.5 nm in size. (b) Selected area diffraction (SAD) pattern showing the lattice fringes of the α-Sn TEM of (a) (unpublished data) (c) Charts showing the position of the α-Sn and β-Sn d-spacings. (Unpublished data.)

Two approaches have been employed in order to form 2D and 3D structures. One is to allow the nanoclusters to self-assemble from dilute solution by depositing a few drops of the solution of clusters on a substrate or by dipping the TEM grid into the dispersion.[19,104,110] Recently, the formation of 2D Au and Ag monolayers using such self-assembly techniques have been reported. Another approach is to use external forces to obtain the nanoparticle monolayers, such as an electrophoretic deposition, [111] or Langmuir–Blodgett film formation.[112] Giersig and Mulvaney demonstrated that the electrophoretic deposition is a useful technique for achieving the 2D organization of Au nanoparticles of various sizes onto a carbon-coated TEM grid.[111,113]

Arrays of hexagonally or cubic close packed quasi-mono-disperse spherical colloids (also known as, quantum dots or nanocluster arrays) can form readily on various types of substrates upon drying from the liquid phase. There are several factors that affect the quality of the final cluster film such as the initial cluster concentration, the drying rate, the type and physical size of organic ligand "shell", and the cluster core

size. As in bulk crystallization, defects and voids could be introduced if the drying rate is too rapid, causing the colloids to be trapped in metastable positions. So, slow drying is favored if a multiple layer, ordered 3-D supracrystal is desired, while a faster drying rate favors monolayer films.

One of the first reports of Au nanocluster superlattice formation was in 1993 by Giersig and Mulvaney.[111] They used a modified version of the classical Faraday synthesis in water to produce ~14 nm diameter clusters. These colloidal samples were charged stabilized with citrate ions, allowing them to use electrophoretic deposition for the formation of monolayer arrays.

Brust et al. used an inverse micelle method with alkane thiols to make arrays of 8 nm Au particles cross-linking them with a bi-functional dithiol.[114] Self-organization of Au nanoparticles without the use of thiols was reported by Fink et al.[115] One of the first groups to report formation of cluster arrays with relatively small Ag nanoparticles was the Whetten group at Georgia Tech.[110] They used surfactant-mediated growth with large amounts of thiol present during the reduction in order to

severely limit the cluster growth. They also showed 3-D superlattices of significant ($\sim$1–10 micron) size. Other groups later also showed the formation of 2-D and 3-D superlattices of Ag.[19,116] Work by Heath and co-workers utilizing inverse micelle techniques produced highly polydisperse dedecanthiol capped Au clusters which still formed ordered arrays. They noted that size exclusion of smaller clusters occurred spontaneously during the drying process.[117] This is why conclusions regarding cluster monodispersity based upon TEM observations in limited areas of the grid are suspect.

It is possible to make nanoalloy films consisting of Au and Ag particles whose relative size ratio allows packing in the form of either AB or AB2 type alloys. Kiely and co-workers describe such arrays in several references.[118,119] A strange aspect of these arrays is that a ratio of Au : Ag of at least 10 : 1 was necessary to observe these ordered regions. Of course, the vast majority of the TEM grid shown consisted of disordered structures, so formation of such complete films is not developed. It would be interesting to study the optical properties of such films, if methods for their uniform formation could be developed.

To obtain more homogeneous films for the purpose of studying their collective optical properties, Ung et al developed methods of coating Au clusters with shells of SiO_2 of controlled thickness.[120] The core size of the Au clusters was determined by the limitations of the Faraday synthesis in aqueous solution and so was fixed at around 15 nm. Variation of the SiO_2 shell thicknesses allowed them to vary the dipole interactions between particles without significant electronic coupling. TEMs showed that there were significant regions of the TEM grid containing no particles, so the models they utilized which assume homogeneity of the films in the illuminated regions may not be appropriate to the samples investigated. With this caveat in mind, a general trend in the peak plasmon absorbance was found for several cluster packing volume fractions. As the interparticle spacing was reduced by decreasing the SiO_2 shell thickness, thus increasing the dipole–dipole interactions, a red shift in the plasmon peak absorbance was found. This agrees with our observations of Au cluster films spray coated onto glass slides.[121] As more layers of clusters were deposited, a blue shift occurred for a fixed interparticle spacing. Simple models described these effects adequately which is surprising given the significant inhomogeneity in the film structure shown in low resolution TEM.

It is also interesting to investigate the effects of metal ligand binding strength on nanocluster array stability. SEC shows that alkylthiols bind more strongly to Au and Pt nanoclusters of a fixed size than to Ag. As a result, Au nanoarrays are more stable under TEM vacuum and imaging conditions compared to Ag nanoarrays. Both Au and Ag initially form large, highly ordered hexagonal arrays as observed in TEM, but the Ag arrays deteriorate in less than 1 day due to alkylthiol desorption followed by cluster fusion or sintering. Unfortunately, this reality is not often discussed in the literature.

As described above, SEC shows that the alkyl chain length plays a role in the binding affinity of metal nanocluster to thiol surfactants. Generally, longer chain length thiols bind more

strongly to Au nanoclusters. Nanocluster array TEM studies as a function of alkyl chain length k show that short chain length, $k < 8$, thiols do not form large ordered domains. An optimal value, $k = 10$–14, for array formation was observed. However, a value of $k = 16$ led to poor array formation despite stronger binding affinity as shown by SEC studies. This contradiction could be resolved by assuming easier alkane chain interdigitation between ligated clusters in the length range $k = 10$–14 favoring array formation.

The drying rate and concentration of the initial cluster solution is also an important factor in determining the structure of the final nanocluster array. Faster drying and lower initial concentration favors the formation of monolayers of hexagonally or square packed nanoclusters, while higher concentrations and slower drying (less volatile solvents) favors cluster pile-up and formation of bilayers along with 3-D crystals on the substrate.

Substrates such as Teflon are more effective than glass for the formation of large ($\sim$10–100 μm), supracrystals. Fig. 29 shows an example of a 3-D superlattice.[94] As can be seen from
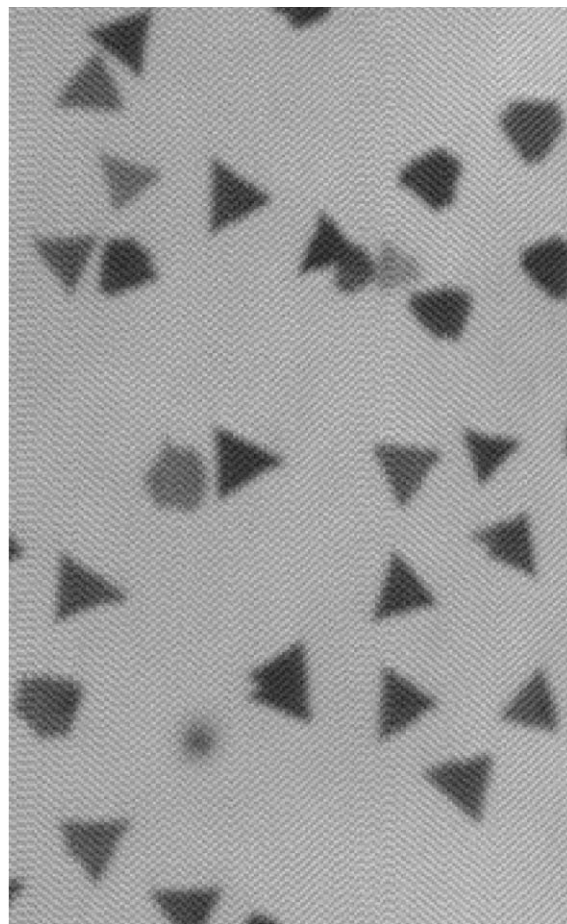

Fig. 29 Optical micrograph of 3-D superlattice nanocluster arrays made of Au nanocrystals with $D_c \sim 4.6$ nm. (Reprinted with permission from ref. 94: from "Quantum Dots Made of Metals: Preparation and Characterization", by J. P. Wilcoxon, in *Dekker Encyclopedia of Nanoscience and Nanotechnology*, Taylor and Francis, 2004, pp. 3177–3202. Copyright (2004) Routledge/Taylor & Francis Group, LLC.)
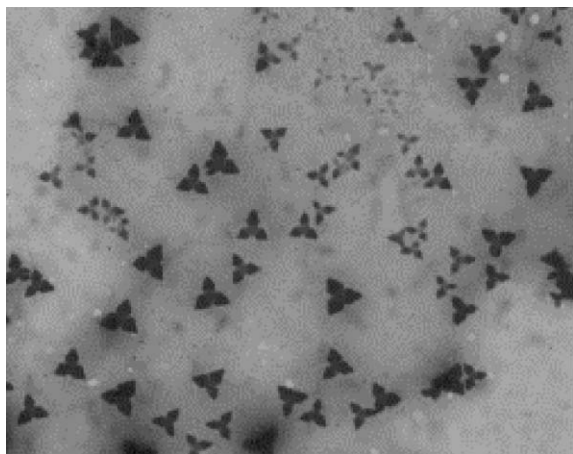
Fig. 30 A tri-foil crystal motif is observed in an optical micrograph of $D_c = 4.0$ Pt supracrystals. It is reminiscent of a well known Japanese corporate logo (though no funding was provided to influence this fortuitous observation). (Reprinted with permission from ref. 94: from ''Quantum Dots Made of Metals: Preparation and Characterization'', by J. P. Wilcoxon, in *Dekker Encyclopedia of Nanoscience and Nanotechnology*, Taylor and Francis, 2004, pp. 3177–3202. Copyright (2004) Routledge/Taylor & Francis Group, LLC.)

this figure, these nanocluster supracrystals formed triangular facets which appear to depend on the nanocrystal core size. Other substrates such as graphite were too porous for good nanocluster array superlattice formation. Holey carbon TEM grids, also relatively porous, favored the formation of either mono- or bi-layer arrays.

The nanocluster arrays formed different habits depending on the metal type and cluster size. Fig. 30 shows the 3-D array formed by 4.0 nm Pt nanocrystals.[94] The "Mitsubishi" motif exhibited by these crystals is quite different compared 2.5 nm Pt nanoclusters (Fig. 31). For both the 4 nm and 2.5 nm Pt
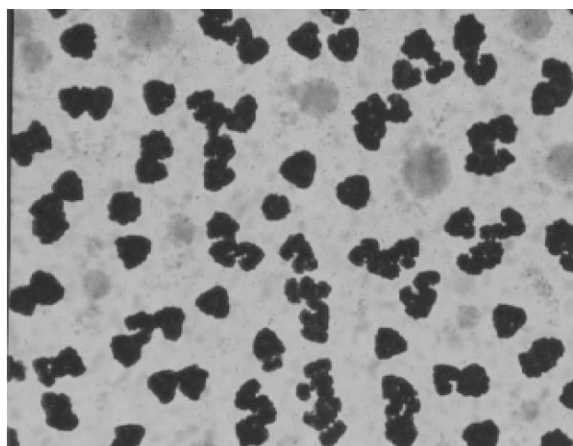

Fig. 31 An optical micrograph is Pt supracrystals formed by very small, $D_c = 2.5$ nm nanocrystals with slightly irregular shapes shows that crystal habit depends on the nanocrystal core size. (Reprinted with permission from ref. 94: from ''Quantum Dots Made of Metals: Preparation and Characterization'', by J. P. Wilcoxon, in *Dekker Encyclopedia of Nanoscience and Nanotechnology*, Taylor and Francis, 2004, pp. 3177–3202. Copyright (2004) Routledge/Taylor & Francis Group, LLC.)
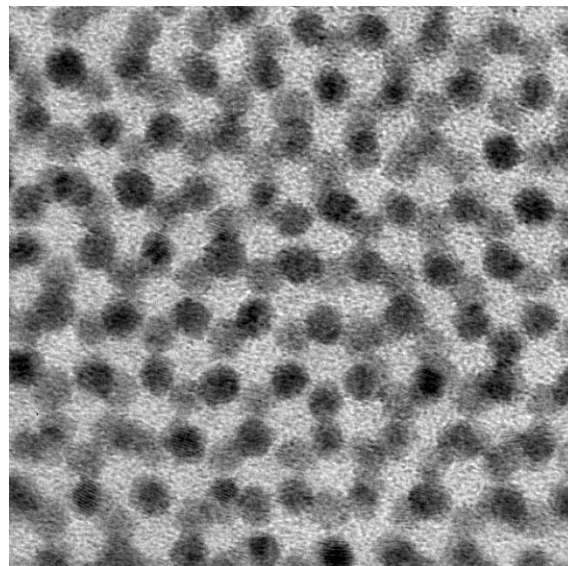

Fig. 32 Pt nanocluster array bilayer with the clusters deposited onto the low energy trigonal sites above the first monolayer. (Reprinted with permission from ref. 122: J. E. Martin, J. P. Wilcoxon, J. Odinek and P. Provencio, Superlattices of platinum and palladium nanoparticles. *J. Phys. Chem. B*, 2002, **106**(5), 971–8. Copyright 2002 American Chemical Society.)

clusters, dodecanthiol was used to passivate the surface, decane was used as the solvent and an identical Pt concentration and substrate was used.

Interesting packing patterns can also occur in bilayers like the ones shown in the Pt TEM images of Fig. 32 and 33.[122] Fig. 32 shows a Pt nanoarray in the form of a bilayer where the low-energy trigonal locations of the second layer are located
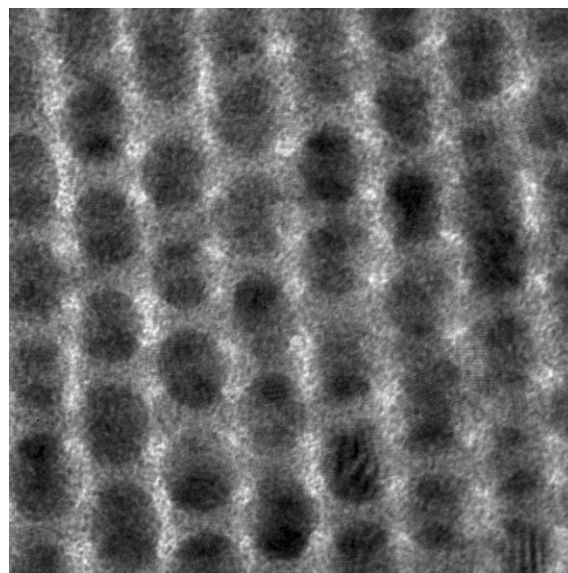

Fig. 33 Pt nanocluster bilayer has the second layer of clusters deposited onto two-fold symmetry sites. (Reprinted with permission from ref. 122: J. E. Martin, J. P. Wilcoxon, J. Odinek and P. Provencio, Superlattices of platinum and palladium nanoparticles. *J. Phys. Chem. B*, 2002, **106**(5), 971–8. Copyright 2002 American Chemical Society.)

above the holes in the first layer. However in Fig. 33, the nanoclusters in the second bilayer occupy two-fold sites.

Less work has been done concerning the differences between the magnetic response behavior of arrays of metal clusters. Petit et al.[98] formed arrays of Co clusters by self-assembly on a TEM or graphite grid and compared them to the same clusters in dispersed form. Surprisingly, both the blocking temperature and magnetic saturation values were nearly the same for the individual clusters dispersed in pyridine as for the ordered arrays. The main effect observed was a larger remnant field in the arrays which seems reasonable due to the dipole coupling between closely packed particles. This causes the value of the local field to exceed that of the imposed external field. And this local field is what affects the response of a given nanoparticle. Why this same coupling did not increase the blocking transition temperature very much remains unexplained? It should be noted that the array packing was fairly defective (i.e. inhomogeneous) so not every particle had adjacent neighbors with which to interact. In our experience, packing Fe clusters into arrays increases the blocking transition temperature by as much as 200 °K compared to individual, dilute clusters of the same size. More experiments on homogeneous arrays are necessary to resolve these disparate behaviors.

As the quality and variety of nanocrystals available to researchers improves there have been recent reports of relatively high quality 3-D nanocrystals formed by self-assembly of both semi-conductor and metal nanoclusters. Shevchenko, Talapin, Murray and O'Brien, for example, describe structural studies using TEM and SAD of binary nanoparticle superlattices with various combinations of metals and semiconductor nanocrystals.[123] In these binary materials, correct selection of the drying conditions, ligands, and nanocluster size ratios allowed superlattices to form in a variety of structural motifs including AB, AB2, AB3, AB4, AB5, AB6, and even AB13 stoichiometry. Cubic, hexagonal tetragonal and orthorhombic symmetries were shown. They showed that electrical charges on sterically stabilized nanoclusters could aid the assembly process. The ligands still need to be present, however, to allow interdigitation of chains to aid the assembly process. Growing such supracrystals consisting of nanoparticles is very much an art as in conventional crystal growth. The lateral domains of their best superlattices were only 3 × 3 mm, with thicknesses of 4–6 layers, so technical applications would be quite limited. They point out that the distinct optical and magnetic properties of the individual nanocluster components might allow what they refer to as "metamaterials" with tunable optical and magnetic properties.

Possible applications and future directions for metal nanoclusters

There are many possible applications for metal nanoclusers, core/shell and alloy structure as well as arrays and super-lattices. The success of these applications in areas such as taggant technology, anti-counterfeiting, radiation detection, magnetism, catalysis, and optics will depend on the choice of material composition, size, and surface chemistry. Nanoclusters will be a small fraction of the volume for these novel composite materials and the clusters will have to be chemically compatible with conventional materials which will provide both the connection to the macroscopic world and the structural support for the clusters. An obvious advantage of incorporation of minute amounts of clusters with unique chemical and physical functions into conventional materials will be lower cost. Since interaction or communication between the clusters and their surroundings occurs at the nanocluster interface, clusters with enormous surface/volume ratios require much less material than their micron size counterparts. This will be true for all the applications to be discussed and is a significant cost advantage as less nanocluster material will be required.

In electronic technology applications of clusters the "wiring" problem of interfacing clusters to the macroscopic world has proved quite formidable. The analogy to the utility of a single transistor compared to arrays of interconnected transistors (e.g. microprocessors, memory etc.) is apt. For example, in proposed light emitting devices based upon fluorescent nanoclusters, injecting electrons and holes into the semiconductor clusters efficiently and without irreversible chemical changes (e.g. oxidation) of the clusters has not been overcome. This is at least partly due to the fact that the "wires" used for this process must have length scales comparable to that of the clusters and so conducting polymers have been the only materials used in prototypes. Undoubtedly, a hierarchy of conducting materials with length scales from the nm to mm will have to be constructed to enable such devices.

Similar difficulties in efficient transfer of charge carriers from nanosize clusters to macrosize devices exist in photo-voltaic applications. In photoelectrochemical cells based upon nanophase TiO_2, for example, scattering of the photogenerated carriers at defects reduces device efficiency much below that of even polycrystalline Si, much less single crystal Si photovolaics. However, as experience grows we may hope improvements in nanomaterials will close this efficiency gap. Whether the cost gap can be overcome is moot as processes for scaling up the synthesis of many nanosize materials are still being developed. The cost of current processes may be judged by the fact that commercially available samples of semiconductor nanocrystals such as CdSe sell for ~$50 K per gram, well above even single walled nanotubes. The resistance to chemical degradation of most nanoclusters to ordinary atmospherical environments also needs substantial improvement. Degradation of many nanocluster materials would have significant environmental impact and this issue needs further examination as companies emerge selling nanocluster-based products.

Also mentioned often in electronic applications of clusters are reduced size computational devices. It is assumed the architecture of these devices will follow that of the microelectronic devices used in present digital computers. However, the "wiring" of such devices on the nanoscale may prove impossible. Instead, one should consider the functioning of analogue computers such as the brain where interactions between chemicals (e.g. neurotransmitters, neutron receptors) induce a detectable change in state which influences the flow of information. This analogy may prove much more useful, but requires reconsideration of the conventional binary logic and connectivity methods of conventional microelectronics. Thus, many of the well-developed manufacturing processes used in

microelectronics fabrication will be inappropriate for nanomaterials.

High density magnetic storage is a strong motivating factor for research aimed at the formation of high coercivity FePt nanocluster arrays.[64] A roadblock to this technology development is our ability to produce the desired anisotropic L_o nanophase in individual clusters. Currently, only a disordered fcc phase has been obtained.[10] Obtaining large regions of defect-free oriented magnetic clusters is also a formidable obstacle to use of clusters in magnetic storage. Technologies which exploit the enhanced magnetic response with no hysteresis of some of the nanosized metals like Fe and Co include magnetic refrigeration, and transformers with little to no losses.

We have extensively discussed the unique optical properties of Au, Ag and nanoalloys thereof. A simple use of such materials to provide unique identifiers for controlled materials is possible. When used as taggants in such an application it is possible to give a material a unique optical signature which depends on nanocluster size, composition and shape. Similar to the metal wires embedded in modern currency, such metal clusters would prove very difficult to duplicate based upon conventional compositional analysis even using advanced instruments available elsewhere in the world. Even if their composition or size could be learned, the order of their construction (e.g. Au/Ag vs Ag/Au vs alloy) would make the duplication of their collective optical absorption properties impossible.

Similarly, the unique magnetic response of superparamagnetic clusters could be used in anti-counterfeiting or tracing controlled materials from production to final utilization, thus avoiding diversion to other uses. Superparamagnetic clusters are already used when linked to antibodies to select out antigens from complex mixtures. In this application, magnetic separation using simple permanent magnets permits purification and further analysis of these proteins.

It has been proposed that arrays of metal nanoclusters could be used as optical waveguides. Here, the concentration of a light wave impinging on a linear array of Au or Ag clusters could be used to confine the light to a dimension much smaller than conventional dielectric waveguides. The light could even be generated using a fluorescent semiconductor cluster in close proximity. The plasmon wave would propagate via successive interaction down the chain of nanoclusters. Applications in this area have been named plasmonics. This focusing of the electro-magnetic field in a small region of space by a metal nanoparticle can also aid in near field probe optical excitation and imaging of molecules and nanostructures. It is already used in surface enhanced Raman scattering experiments to sensitively detect organic molecules adsorbed to fractal metal aggregates of Au, Ag, and Cu.

Metal nanoclusters are likely to have their most significant near-term impact in the field of chemistry, particularly catalysis. Fe and FeS_2 nanoclusters can act as coal hydrogenation and hydrogenolysis catalysts. These nanoclusters are directly deposited onto the coal powder, which acts both as a support and a substrate.[124] Co or Ni nanoclusters could play an important role in enhancing the activity of catalysts such as MoS_2 in fuel refining. In this application heteroatomic molecules such a thiols or amines, present in crude oil are removed to prevent poisoning of expensive metal catalysts used in subsequent fuel refining steps.

Nanosized metals generated by the synthesis protocols described in this review have not been utilized as catalysts because of concerns regarding the effect of the ligand used in the synthesis on substrate binding. However, their small size and large surface area can transform some of the most unlikely materials into catalysis candidates. This was shown by Haruta et al when they demonstrated that Au nanoparticles were active at room temperature in the oxidation of carbon monoxide to carbon dioxide.[125] This novel use of Au clusters as CO oxidation catalysts could possibly be utilized in the purification of H_2 used in fuel cells where poisoning of the fuel cell Pt electrocatalyst by CO present in the hydrogen gas stream (from the syn-gas process) is a major problem.

Pd, Pt, and Rh nanoclusters deposited on high surface area, commercially available supports such as alumina and carbon lead to milder T and P conditions for hydrogenation. An example is shown in the unpublished data of Fig. 34 where Pd clusters are actually more active than more expensive Pt and Rh clusters. The conditions of temperature and pressure shown in this figure are also quite mild compared to that required by commercial catalysts on the same high surface area support. Also, the product distribution (selectivity) can be tuned by nanocluster size and metal type.

Another application of metal nanocluster is as electrocatalysts where there is a need to replace the expensive Pt electrocatalysts currently being used. Alloys of more inexpensive metals incorporating Fe, Mo or their metal sulfides may be candidates. The possibilities for metal nanoclusters in this field of catalysis are significant since they are already used in less controlled form as conventional heterogeneous catalysts. New combinations of metals will likely be useful since the interatomic spacing at the surface of 2–3 nm clusters can be different from conventional materials and subject to control by the nanoalloying process described in this review.
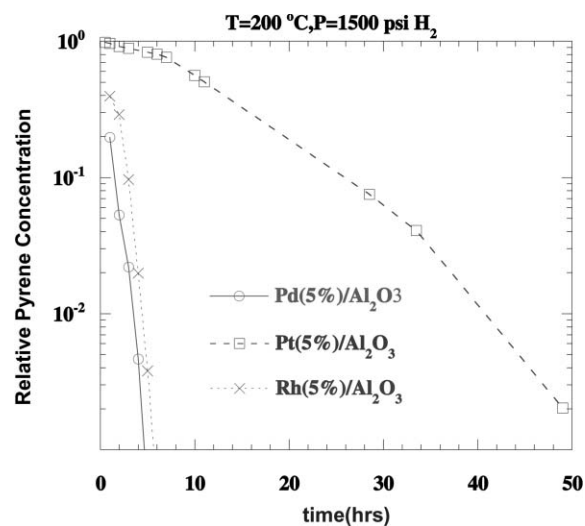

Fig. 34 Pyrene hydrogenation as a function of reaction time under the reaction conditions indicated. Equal weight fractions of Pd, Pt and Rh clusters with sizes around 2–3 nm were deposited onto commercial high surface area alumina, Al_2O_3 support (400 g m^{-2}). (Unpublished data.)

This journal is © The Royal Society of Chemistry 2006

Chem. Soc. Rev., 2006, **35**, 1162–1194 | 1191

Conclusions

In this review we discussed three methods for the synthesis of metal nanoclusters. All three methods depend on ligand stabilization for the control of the average cluster size and size dispersion. Inverse micelle synthesis in non-polar oils using readily available, inexpensive, ionic metal salts encapsulated in the micelle hydrophilic interior is the most versatile, safe, and scalable method for metal nanocluster synthesis. Reduction of metal salts using alcohols or glycols was described and examples of transition metal, Pt and Pd clusters as well as base metal Fe, Co and Ni cluster synthesis were discussed. Thermal decomposition of metal-organic precursors in the presence of polymers was shown to be useful for larger, $d > 3$ nm, clusters of Co, Fe and Ni, but sometimes results in disordered clusters with structures different from the bulk material. In this context, the role of the surfactant in control of the final nanostructure was discussed for Co, Fe, and Sn. We demonstrated the use of size-exclusion chromatography, SEC, for cluster size analysis and the role such rapid feedback plays in synthesis development. We demonstrated that special, thermodynamically stable cluster sizes are formed in the size regime $D_c < 3$ nm, that the binding strengths of ligands to metal nanoclusters is stronger for Au than Ag, and that longer chain length thiols have larger binding affinity. We noted that short chain length alkyl thiols can etch solutions of poly-disperse clusters, transferring atoms from larger to smaller clusters and reducing the width of size distribution with sample age.

The use of small seed clusters to grow successive generations of homo- and heteroatomic clusters was discussed. The use of SEC to follow this growth process was given as an example. This analytical method allowed us to determine the size-dependent optical properties of both core/shell and nanoalloy particles of Ag and Au. The feedback provided by SEC was critical to the development of the synthesis protocol.

The optical properties of core-shell particles of equivalent size and atomic composition was shown to depend on whether Ag or Au was in the interior and was further shown to depend on whether an alloy or core-shell structure was formed.

We next discussed the various synthetic approaches and resulting magnetic properties of nanoclusters of Co, Fe, and Ni. We demonstrated that restructuring of the clusters in solution could increase the magnetic response with age resulting in a magnetic response greater than bulk Co. The effects of surfactants on the magnetic properties were significant but poorly understood. The surface magnetism and surface reconstruction in small nanocrystals could explain some of our observations. It was also shown that super-paramagnetic core/shell Fe/Ag and Fe/Pt nanoparticles have reduced saturation magnetism compared to alloys of the same composition and size but that alloys of the same composition and similar size have superior magnetic properties.

A discussion of cluster matter consisting of arrays of nanocrystals of Au, Pt, and Pd followed. We summarized the important parameters controlling the degree of order and whether mono- bi- or multilayer arrays (superlattices) are observed. We gave examples showing that nanocluster bi-layers of Pt may exhibit either the predicted low energy three-fold co-ordination or a two-fold coordination in the second layer. We also summarized the most recent synthetic developments in the field.

We concluded our review with a discussion of the possible applications of metal nanoclusters, emphasizing their unique size and surface chemistry properties. Tuning of the size, shape, and interface structure of nanoclusters is critical to their utilization in applications such as new magnetic, dielectric, optical, and catalytic materials.

Acknowledgements

References

1 L. M. Liz-Marzan, *Langmuir*, 2006, **22**, 32.
2 J. Rodriguez-Fernandez, J. Perez-Juste, F. J. Garcia de Abajo and L. M. Liz-Marzan, *Langmuir*, 2006, **22**, 7007.
3 W. A. de Heer, *Rev. Mod. Phys.*, 1993, **65**, 611.
4 M. Faraday, *Philos. Trans. R. Soc. London*, 1857, **Part I**, 145.
5 U. Kreibig and M. Vollmer, *Optical Properties of Metal Nanocluster*, ed. J. P. Toennies, Springer, Berlin, 1995.
6 S. R. Hoon, M. Kilner, G. J. Russell and B. K. Tanner, *J. Appl. Polym. Sci.*, 1966, **10**, 1915.
7 C. H. Griffiths, M. P. O'Horo and T. W. Smith, *J. Appl. Phys.*, 1979, **50**, 7108.
8 P. Hess and J. P. S. Parker, *J. Appl. Polym. Sci.*, 1966, **10**, 1915.
9 C. B. Murray, S. H. Sun, H. Doyle and T. Betley, *MRS Bull.*, 2001, **26**, 985.
10 S. Sun, C. B. Murray, D. Weller, L. Folks and A. Moser, *Science*, 2000, **287**, 1989.
11 G. Schmid, *Angew. Chem.*, 1978, **90**, 417.
12 J. D. Aiken and R. G. Finke, *J. Mol. Catal. A: Chem.*, 1999, **145**, 1.
13 G. Schmid, *Developments in Transition Metal Cluster Chemistry – The Way to Large Clusters. Structure and Bonding*, Springer-Verlag, Berlin, 1985.
14 N. Pradhan, N. R. Jana, K. Mallick and T. Pal, *J. Surf. Sci. Technol.*, 2000, **16**, 188.
15 M. Boutonnet, J. Kizling and P. Stenius, *Colloids Surf.*, 1982, **5**, 209.
16 M. Boutonnet, J. Kizling, V. Mintsa-Eya, A. Choplin, R. Touroude, G. Maire and P. Stenius, *J. Catal.*, 1987, **103**, 95.
17 P. Calandra, C. Giodano, A. Longo and V. T. Liveri, *Mater. Chem. Phys.*, 2006, **98**, 494.
18 M. P. Pileni, B. Hickel, C. Ferradini and J. Pucheault, *Chem. Phys. Lett.*, 1982, **92**, 308.
19 A. Taleb, C. Petit and M. P. Pileni, *Chem. Mater.*, 1997, **9**, 950.
20 P. Lianos and J. K. Thomas, *Chem. Phys. Lett.*, 1986, **125**, 299.
21 M. L. Steigerwald, A. P. Alivisatos, J. M. Gibson, T. D. Harris, R. Kortan, A. J. Muller, A. M. Thayer, T. M. Duncan, D. C. Douglass and L. E. Brus, *J. Am. Chem. Soc.*, 1988, **110**, 3046.
22 C. B. Murray, C. R. Kagan and M. G. Bawendi, *Annu. Rev. Mater. Sci.*, 2000, **30**, 545.
23 J. P. Wilcoxon, Method for the Preparation of Metal Colloids in Inverse Micelles and Product preferred by the method, *US Pat.*, 5,147,841, 1992.
24 J. P. Wilcoxon, R. L. Williamson and R. Baughman, *J. Chem. Phys.*, 1993, **98**, 9933.

25 J. P. Wilcoxon, P. P. Provencio and G. A. Samara, *Phys. Rev. B: Condens. Matter*, 2001, **64**, 035417.
26 J. P. Wilcoxon, G. A. Samara and P. N. Provencio, *Phys. Rev. B: Condens. Matter*, 1999, **60**, 2704.
27 M. Brack, *Rev. Mod. Phys.*, 1993, **65**, 677.
28 G. Friedlander, J. W. Kennedy and J. M. Miller, *Nuclear and Radiochemistry, 2nd Edn*, John Wiley & Sons, New York, 1966.
29 W. Ekardt, *Phys. Rev. B: Condens. Matter*, 1984, **29**, 1558.
30 I. M. L. Billas, A. Chatelain and W. A. De Heer, *J. Magn. Magn. Mater.*, 1997, **168**, 64.
31 L. Brus, *J. Phys. Chem.*, 1986, **90**, 2555.
32 C. H. Fischer, H. Weller, L. Katsikas and A. Henglein, *Langmuir*, 1989, **5**, 429.
33 A. Fojtik, H. Weller, U. Koch and A. Henglein, *Ber. Bunsen-Ges. Phys. Chem.*, 1984, **88**, 969.
34 Z. Zhou, L. Brus and R. Friesner, *Nano Lett.*, 2003, **3**, 163.
35 Z. Zhou, R. A. Friesner and L. Brus, *J. Am. Chem. Soc.*, 2003, **125**, 15599.
36 J. Osuna, D. deCaro, C. Amiens, B. Chaudret, E. Snoeck, M. Respaud, J. M. Broto and A. Fert, *J. Phys. Chem.*, 1996, **100**, 14571.
37 B. Chaudret, *C. R. Phys.*, 2005, **6**, 117.
38 O. Margeat, F. Dumestre, C. Amiens, B. Chaudret, P. Lecante and M. Respaud, *Prog. Solid State Chem.*, 2005, **33**, 71.
39 E. V. Shevchenko, D. V. Talapin, H. Schnablegger, A. Kornowski, O. Festin, P. Svedlindh, M. Haase and H. Weller, *J. Am. Chem. Soc.*, 2003, **125**, 9090.
40 H. Bonnemann and R. M. Richards, *Eur. J. Inorg. Chem.*, 2001, 2455.
41 P. M. Mendes, Y. Chen, R. E. Palmer, K. Nikitin, D. Fitzmaurice and J. A. Preece, *J. Phys.: Condens. Matter*, 2003, **15**, S3047.
42 A. J. Quinn and G. Redmond, *Prog. Solid State Chem.*, 2005, **33**, 263.
43 J. P. Wilcoxon and P. N. Provencio, *J. Phys. Chem. B*, 1999, **103**, 9809.
44 J. P. Wilcoxon and P. Provencio, *J. Phys. Chem. B*, 2003, **107**, 12949.
45 A. Henglein, *Top. Curr. Chem.*, 1988, **143**, 113.
46 C. W. W. Ostwald, *An Introduction to Theoretical and Applied Colloid Chemistry, 'The World of Neglected Dimensions'*, John Wiley & Sons, New York, 1917.
47 L. Ratke and P. W. Vorhees, *Growth and Coarsening Ostwald Ripening in Materials Processing*, Springer-Verlag, Berlin, 2002.
48 J. P. Wilcoxon and R. L. Williamson, *Mater. Res. Soc. Symp. Proc.*, Boston, MA, 1989, p. 269.
49 T. G. Schaaff and R. I. Whetten, *J. Phys. Chem. B*, 1999, **67**, 3021.
50 S. Stoeva, K. J. Klabunde, C. Sorensen and I. Dragieva, *J. Am. Chem. Soc.*, 2002, **124**, 2305.
51 R. L. Whetten, J. T. Khoury, M. M. Alvarez, S. Murthy, I. Vezmar, Z. L. Wang, P. W. Stephens, C. L. Clevelend, W. D. Luedtke and U. Landman, *Adv. Mater.*, 1996, **8**, 428.
52 J. P. Wilcoxon, J. E. Martin and P. Provencio, *Langmuir*, 2000, **16**, 9912.
53 M. Brust, J. Fink, D. Bethell, D. J. Schriffin and C. Kiely, *J. Chem. Soc., Chem. Commun.*, 1995, 1655.
54 H. Hirai, Y. Nakao and N. Toshima, *J. Macromol. Sci., Chem.*, 1978, **A12**, 1117.
55 J. S. Bradley, J. M. Millar and E. W. Hill, *J. Am. Chem. Soc.*, 1991, **113**, 4016.
56 J. S. Bradley, E. W. Hill, C. Klein, B. Chaudret and A. Duteil, *Chem. Mater.*, 1993, **5**, 254.
57 D. Zitoun, M. Respaud, M. C. Fromen, P. Lecante, M. J. Casanove, C. Amiens and B. Chaudret, *J. Magn. Magn. Mater.*, 2004, **272–276**, 1536.
58 A. Rodriguez, C. Amiens, B. Chaudret, M. J. Casanove, P. Lecante and J. S. Bradley, *Chem. Mater.*, 1996, **8**, 1978.
59 T. O. Ely, C. Amiens, B. Chaudret, E. Snoeck, M. Verelst, M. Respaud and J. M. Broto, *Chem. Mater.*, 1999, **11**, 526.
60 C. Pan, K. Pelzer, K. Philippot, B. Chaudret, F. Dassenoy, P. Lecante and M. J. Casanove, *J. Am. Chem. Soc.*, 2001, **123**, 7584.
61 D. Wostek-Wojciechowska, J. K. Jeska, C. Amiens, B. Chaudret and P. Lecante, *J. Colloid Interface Sci.*, 2005, **287**, 107.
62 T. Teranishi, M. Hosoe, T. Tanaka and M. Miyake, *J. Phys. Chem. B*, 1999, **103**, 3818.
63 T. Teranishi and M. Miyake, *Chem. Mater.*, 1998, **10**, 594.
64 D. Farrell, S. A. Majetich and J. P. Wilcoxon, *J. Phys. Chem. B*, 2003, **107**, 11022.
65 Z. A. Peng and X. G. Peng, *J. Am. Chem. Soc.*, 2002, **124**, 3343.
66 B. O. Dabbousi, J. Rodriguez-Viejo, F. V. Mikulec, J. R. Heine, H. Mattoussi, R. Ober, K. F. Jensen and M. G. Bawendi, *J. Phys. Chem. B*, 1997, **101**, 8455.
67 C. B. Murray, D. J. Norris and M. G. Bawendi, *J. Am. Chem. Soc.*, 1993, **115**, 8706.
68 D. J. Norris, A. Sacra, C. B. Murray and M. G. Bawendi, *Phys. Rev. Lett.*, 1994, **101**, 8455.
69 X. G. Peng, M. C. Schlamp, A. V. Kadavanich and A. P. Alivisatos, *J. Am. Chem. Soc.*, 1997, **119**, 7019.
70 J. P. Wilcoxon and P. P. Provencio, *J. Am. Chem. Soc.*, 2004, **126**, 6402.
71 L. Brus, *J. Phys. Chem. Solids*, 1998, **59**, 459.
72 K. A. Littau, P. J. Szajowski, A. J. Muller, A. R. Kortan and L. E. Brus, *J. Phys. Chem.*, 1993, **97**, 1224.
73 J. P. Wilcoxon and S. A. Craft, *Nanostructured Materials, Third International Conference on Nanostructured Materials, 8–12 July 1996, Kona, HI, USA*, 1997, **9**, 85.
74 W. W. Yau, J. J. Kirkland and D. D. Bly, *Modern Size-Exclusion Liquid Chromatography*, Wiley-Interscience, New York, 1979.
75 J. P. Wilcoxon, J. E. Martin, F. Parsapour, B. Wiedenman and D. F. Kelley, *J. Chem. Phys.*, 1998, **108**, 9137.
76 S. Link, A. Beeby, S. Fitzgerald, M. A. El-Sayed, T. G. Schaaff and R. I. Whetten, *J. Phys. Chem. B*, 2002, **106**, 3410.
77 T. G. Schaaff, M. N. Shafigullin, J. T. Khoury, I. Vezmar, R. I. Whetten, W. G. Cullen, P. N. First, C. Gutierrex-Wing, J. Ascnisio and M. J. Jose-Yacaman, *J. Phys. Chem. B*, 1997, **101**, 7885.
78 J. P. Wilcoxon, S. A. Craft and T. R. Thurston, *Rev. Sci. Instrum.*, 9th National Conference on Synchrotron Radiation Instrumentation, 1996, p. 3021.
79 J. P. Wilcoxon, J. E. Martin and P. Provencio, *J. Chem. Phys.*, 2001, **115**, 998.
80 U. Kreibig and L. Genzel, *Surf. Sci.*, 1985, **156**, 678.
81 G. Mie, *Ann. Phys.*, 1908, **25**, 377.
82 A. Henglein, *Chem. Rev.*, 1989, **89**, 1861.
83 P. V. Kamat and D. Meisel, *Curr. Opin. Colloid Interface Sci.*, 2002, **7**, 282.
84 W. X. Zhang, *J. Nanopart. Res.*, 2003, **5**, 323.
85 P. Mulvaney, M. Giersig and A. Henglein, *J. Phys. Chem.*, 1993, **97**, 7061.
86 M. A. Watzky and R. G. Finke, *Chem. Mater.*, 1997, **9**, 3083.
87 X. M. Lin, C. M. Sorensen, K. J. Klabunde and G. C. Hajapanayis, *J. Mater. Res.*, 1999, **14**, 1542.
88 K. R. Brown, D. G. Walter and M. J. Natan, *Chem. Mater.*, 2000, **12**, 306.
89 N. R. Jana, L. Gearheart and C. J. Murphy, *Langmuir*, 2001, **17**, 6782.
90 S. Link, Z. L. Wang and M. A. El-Sayed, *J. Phys. Chem. B*, 1999, **103**, 3529.
91 K. Mallik, M. Mandal, N. Pradhan and T. Pal, *Nano Lett.*, 2001, **1**, 319.
92 P. Mulvaney, *Langmuir*, 1996, **12**, 788.
93 S. W. Han, Y. Kim and K. Kim, *J. Colloid Interface Sci.*, 1998, **208**, 272.
94 J. P. Wilcoxon, *Dekker Encyclopedia of Nanoscience and Nanotechnology*, Taylor and Francis, New York, 2004, p. 3177.
95 H. Topsøe, *J. Catal.*, 2003, **216**, 155.
96 H. Topsøe, B. S. Clausen, R. Candia, C. Wivel and S. Morup, *J. Catal.*, 1981, **68**, 433.
97 S. Sun and C. B. Murray, *J. Appl. Phys.*, 1999, **85**, 4325.
98 C. Petit, A. Taleb and M. P. Pileni, *J. Phys. Chem. B*, 1999, **103**, 1805.
99 J. P. Wilcoxon, E. L. Venturini and P. Provencio, *Phys. Rev. B: Condens. Matter*, 2004, **69**, 172402.
100 M. Respaud, *J. Appl. Phys.*, 1999, **86**, 555.
101 J. P. Chen, C. M. Sorensen, K. J. Klabunde and G. C. Hadjipanayis, *Phys. Rev. B: Condens. Matter*, 1995, **51**, 11527.
102 P. G. Harrison, in *Chemistry of Tin*, Chapman and Hall, New York, 1989.

This journal is © The Royal Society of Chemistry 2006

Chem. Soc. Rev., 2006, **35**, 1162–1194 | 1193

103 R. W. Smith and F. Vnuk, *Mater. Res. Soc. Symp. Proc., Phase Transformations in Solids, Symposium.; Chania, Gr*, 1984, **21**, 795.
104 R. G. Freeman, K. C. Grabar, K. J. Allison, R. M. Bright, J. A. Davis, A. P. Guthrie, M. B. Hommer, M. A. Jackson, P. C. Smith, D. G. Walter and M. J. Natan, *Science*, 1995, **267**, 1629.
105 A. Kumar and G. M. Whitesides, *Science*, 1994, **263**, 60.
106 Y. Xia, E. Kim, M. Mrksich and G. M. Whitesides, *Chem. Mater.*, 1996, **8**, 601.
107 P. Hinz and H. Dislich, *J. Non-Cryst. Solids*, 1986, **82**, 411.
108 R. E. Hahn and B. O. Seraphin, *Physics of Thin Films*, Academic Press, New York, 1978.
109 M. A. Kastner, *Phys. Today*, 1993, **46**, 24.
110 S. A. Harfenist, Z. L. Wang, M. M. Alvarez, I. Vezmar and R. L. Whetten, *J. Phys. Chem.*, 1996, **100**, 13904.
111 M. Giersig and P. Mulvaney, *J. Phys. Chem.*, 1993, **97**, 6334.
112 F. C. Meldrum, N. A. Kotov and J. H. Fendler, *Langmuir*, 1994, **10**, 2035.
113 M. Giersig and P. Mulvaney, *Langmuir*, 1993, **9**, 3408.
114 M. Brust, D. Berthell, D. J. Schriffin and C. Kiely, *Adv. Mater.*, 1995, 7.
115 J. Fink, C. Kiely, D. Bethell and D. J. Schriffin, *Chem. Mater.*, 1998, 10.
116 A. Taleb, C. Petit and M. P. Pileni, *J. Phys. Chem. B*, 1998, **102**, 2214.
117 J. R. Heath, C. M. Knobler and D. V. Leff, *J. Phys. Chem. B*, 1997, **101**, 189.
118 C. Kiely, J. Fink, M. Brust, D. Bethell and D. J. Schriffin, *Nature*, 1998, **396**, 444.
119 C. Kiely, J. Fink, J. G. Zheng, M. Brust, D. Bethell and D. J. Schriffin, *Adv. Mater.*, 2000, **12**, 640.
120 T. Ung, L. M. Liz-Marzan and P. Mulvaney, *J. Phys. Chem. B*, 2001, **105**, 3441.
121 J. E. Martin, J. Odinek, J. P. Wilcoxon, R. A. Anderson and P. Provencio, *J. Phys. Chem. B*, 2003, **107**, 430.
122 J. E. Martin, J. P. Wilcoxon, J. Odinek and P. Provencio, *J. Phys. Chem. B*, 2002, **106**, 971.
123 E. V. Shevchenko, D. V. Talapin, C. B. Murray and S. Obrien, *J. Am. Chem. Soc.*, 2006, **128**, 3620.
124 J. P. Wilcoxon, A. Sylwester, P. Nigrey, A. Martino, C. Quintana and R. Baughman, Eighth Annual International Pittsburgh Coal Conference Proceedings, 1991, p. 703.
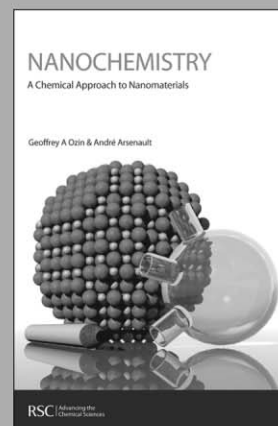125 M. Haruta, *J. Nanopart. Res.*, 2003, **5**, 3.